THE EUROPEAN
PHYSICAL JOURNAL C

A dispersive analysis of $\eta' \to \pi^+\pi^-\gamma$ and $\eta' \to \ell^+\ell^-\gamma$

Simon Holz[1,a] , **Christoph Hanhart**[2] , **Martin Hoferichter**[3,4] , **Bastian Kubis**[1]

[1] Helmholtz-Institut für Strahlen- und Kernphysik and Bethe Center for Theoretical Physics, Universität Bonn, 53115 Bonn, Germany
[2] Forschungszentrum Jülich, Institute for Advanced Simulation, Institut für Kernphysik, and Jülich Center for Hadron Physics, 52425 Jülich, Germany
[3] Albert Einstein Center for Fundamental Physics, Institute for Theoretical Physics, University of Bern, Sidlerstrasse 5, 3012 Bern, Switzerland
[4] Institute for Nuclear Theory, University of Washington, Seattle, WA 98195-1550, USA

Abstract We present a dispersive representation of the η' transition form factor that allows one to account, in a consistent way, for the effects of ρ–ω mixing in both the isoscalar and the isovector contributions. Using this formalism, we analyze recent data on $\eta' \to \pi^+\pi^-\gamma$ to constrain the isovector part of the form factor, individually and in combination with data for the pion vector form factor, which suggests a tension in the ρ–ω mixing parameter. As a first application, we use our results, in combination with the most recent input for the isoscalar part of the form factor, to predict the corresponding spectrum of $\eta' \to \ell^+\ell^-\gamma$, in particular we find the slope parameter $b_{\eta'} = 1.455(24)\,\text{GeV}^{-2}$. With forthcoming data on the latter process, our results establish the necessary framework to improve the evaluation of the η'-pole contribution to the anomalous magnetic moment of the muon using experimental input from both η' decay channels.

1 Introduction

The transition form factors (TFFs) of pseudoscalar mesons, $F_{P\gamma^*\gamma^*}(q_1^2, q_2^2)$ with $P = \pi^0, \eta, \eta'$, describe the interaction with two (virtual) photons,

$$i \int \mathrm{d}^4 x \, e^{iq_1 \cdot x} \langle 0 | T\{j_\mu(x) j_\nu(0)\} | P(q_1 + q_2) \rangle$$
$$= \epsilon_{\mu\nu\alpha\beta} q_1^\alpha q_2^\beta F_{P\gamma^*\gamma^*}(q_1^2, q_2^2), \tag{1.1}$$

where $j_\mu = (2\bar{u}\gamma_\mu u - \bar{d}\gamma_\mu d - \bar{s}\gamma_\mu s)/3$ is the electromagnetic current, $q_{1,2}$ are the photon momenta, and $\epsilon^{0123} = +1$. For both photons on-shell, these form factors determine the di-

photon decays governed by the chiral anomaly [1,2]

$$\Gamma(P \to \gamma\gamma) = \frac{\pi\alpha^2 M_P^3}{4} |F_{P\gamma\gamma}|^2, \tag{1.2}$$

with $F_{P\gamma\gamma} = F_{P\gamma^*\gamma^*}(0, 0)$. For the pion, the corresponding normalization was experimentally [3] found to be close to the prediction from the low-energy theorem [4–6] $F_{\pi^0\gamma\gamma} = 1/(4\pi^2 F_\pi)$ in terms of the pion decay constant F_π, to the extent that higher-order corrections [7–10] thwart agreement with experiment. For $P = \eta, \eta'$ the analog relations depend on the details of η–η' mixing [11–17], see Ref. [18] for a review. Here, we will use the outcome of the PDG global fit, $\Gamma(\eta' \to \gamma\gamma) = 4.34(14)\,\text{keV}$ [19], i.e.,

$$F_{\eta'\gamma\gamma} = 0.3437(55)\,\text{GeV}^{-1}. \tag{1.3}$$

Beyond the normalization, understanding the momentum dependence of the TFFs is critical to be able to calculate the pseudoscalar-pole contributions to hadronic light-by-light scattering (HLbL) in the anomalous magnetic moment of the muon. Currently, the main uncertainty in the Standard-Model prediction [20–48]

$$a_\mu^{\text{SM}} = 116\,591\,810(43) \times 10^{-11} \tag{1.4}$$

originates from hadronic vacuum polarization, see, e.g., Refs. [20,49–54] for further discussion, but to match the final projected precision of the Fermilab experiment, which will improve upon the current world average [55–59]

$$a_\mu^{\text{exp}} = 116\,592\,061(41) \times 10^{-11} \tag{1.5}$$

by more than another factor of two, also the uncertainties in

[a] e-mail: holz@hiskp.uni-bonn.de (corresponding author)

the subleading HLbL contribution, in Ref. [20] estimated as [33–46,60–65]

$$a_\mu^{\text{HLbL}} = 90(17) \times 10^{-11}, \tag{1.6}$$

need to be reduced accordingly. Recent progress includes a second complete lattice calculation [66], while on the phenomenological side the role of higher intermediate states and the implementation of short-distance constraints are being scrutinized [67–75]. Besides these subleading contributions, the η and η' poles are currently estimated using Canterbury approximants alone [37] – as opposed to the π^0 pole, for which independent calculations from dispersion relations [40,41], lattice QCD [42], and Canterbury approximants all give a coherent picture – so that a full dispersive analysis is called for to corroborate the corresponding uncertainty estimates. Several steps in this direction have already been taken in previous work [76–79], in particular, towards a better understanding of the role of factorization-breaking terms [79].

In this paper, we address another subtlety that is related to the interplay of isoscalar and isovector contributions. In principle, since η, η' have isospin $I = 0$, both photons need to be either isoscalar or isovector, leading to a simple vector-meson-dominance (VMD) picture of decays proceedings either via two ρ mesons or some combination of ω and ϕ. However, isospin-breaking effects are resonance enhanced just as in the pion vector form factor (VFF), so that both the admixture of an ω into the isovector contribution and, vice versa, of $\pi\pi$ intermediate states into the isoscalar component can become phenomenologically relevant, at least in the vicinity of the resonance. This issue becomes particularly important when the two-pion cut in the isovector contribution is constrained via data for $\eta' \to \pi^+\pi^-\gamma$, since also in this case isoscalar corrections will enter. Based on Ref. [80] we develop a coupled-channel formalism that allows one to disentangle these effects in a consistent manner, apply the result to recent $\eta' \to \pi^+\pi^-\gamma$ data from BESIII [81], and then calculate the resulting singly-virtual TFF to predict the spectrum for $\eta' \to \ell^+\ell^-\gamma$. A summary of the formalism is given in Sect. 2, with a detailed derivation in the appendix. Fits to the $\eta' \to \pi^+\pi^-\gamma$ data are presented in Sect. 3, followed by the prediction for $\eta' \to \ell^+\ell^-\gamma$ in Sect. 4 and our conclusions in Sect. 5.

2 Formalism

The singly-virtual TFF in the definition (1.1) determines the spectrum for $P \to \ell^+\ell^-\gamma$ according to

$$\frac{\text{d}\Gamma(P \to \ell^+\ell^-\gamma)}{\text{d}s} = \frac{\alpha^3(M_P^2 - s)^3(s + 2m_\ell^2)\sigma_\ell(s)}{6M_P^3 s^2}$$

$$\times \left|F_{P\gamma^*\gamma^*}(s,0)\right|^2, \tag{2.1}$$

where s is the invariant mass of the lepton pair and $\sigma_\ell(s) = \sqrt{1 - 4m_\ell^2/s}$ the phase-space variable. Once $F_{P\gamma^*\gamma^*}(s,0)$ is known, the di-lepton spectrum can thus be predicted.

However, the differential decay width (2.1) scales as $\mathcal{O}(\alpha^3)$ in the fine-structure constant $\alpha = e^2/(4\pi)$, leading to a challenging experimental signature. Additional information on the energy dependence can be obtained by combining the $P \to \pi^+\pi^-\gamma$ decay with the pion VFF F_π^V,

$$\langle \pi^\pm(p')|j^\mu(0)|\pi^\pm(p)\rangle = \pm(p'+p)^\mu F_\pi^V((p'-p)^2), \tag{2.2}$$

which determines the discontinuity of the dominant 2π intermediate states. Experimentally, the decay $P \to \pi^+\pi^-\gamma$ is more easily accessible, given that in this case the differential decay width only scales as $\mathcal{O}(\alpha)$, and information on the spectrum can then be used to reconstruct the isovector part of the TFF. This strategy is straightforward as long as isospin violation is neglected, while the transition from $P \to \pi^+\pi^-\gamma$ to $P \to \ell^+\ell^-\gamma$ becomes more intricate once such corrections are included. In particular, ρ–ω mixing is enhanced by the presence of the resonance propagator, and therefore needs to be included to obtain a realistic line shape. In such a situation, one cannot consider the 2π channel in isolation anymore, since also F_π^V depends on ρ–ω mixing, leading to a spectral function in which the double discontinuities of 2π and 3π intermediate states, corresponding to ρ and ω, respectively, no longer cancel. In Appendix A–Appendix D we systematically develop a formalism that avoids such inconsistencies, allowing for a meaningful consideration of ρ–ω mixing in both the isoscalar and isovector contributions. The central result is given by

$$F_{P\gamma^*\gamma^*}(s,0) = F_{P\gamma\gamma} + \left[1 + \frac{\epsilon_{\rho\omega}s}{M_\omega^2 - s - iM_\omega\Gamma_\omega}\right]$$

$$\times \frac{s}{48\pi^2}\int_{4M_\pi^2}^\infty \text{d}s' \frac{\sigma_\pi^3(s')P(s')|F_\pi^V(s')|^2}{s' - s - i\epsilon}$$

$$+ \frac{F_{P\gamma\gamma}w_{P\omega\gamma}s}{M_\omega^2 - s - iM_\omega\Gamma_\omega}\left[1 + \frac{\epsilon_{\rho\omega}s}{48\pi^2 g_{\omega\gamma}^2}\right.$$

$$\left.\times \int_{4M_\pi^2}^\infty \text{d}s' \frac{\sigma_\pi^3(s')|F_\pi^V(s')|^2}{s'(s' - s - i\epsilon)}\right]$$

$$+ \frac{F_{P\gamma\gamma}w_{P\phi\gamma}s}{M_\phi^2 - s - iM_\phi\Gamma_\phi}, \tag{2.3}$$

a dispersion relation constructed from a spectral function whose double discontinuity vanishes, see Eq. (D.16). Equation (2.3) is expressed in terms of the ρ–ω mixing parameter $\epsilon_{\rho\omega}$ and the weights $w_{PV\gamma}$, defined in Eq. (D.8), which determine the isoscalar contribution to the slope of the TFF, as well as the second-order polynomial

$$P(s) = \frac{A}{2}\left(1 + \beta s + \gamma s^2\right) \tag{2.4}$$

introduced to describe the $\eta' \to \pi^+\pi^-\gamma$ decay spectrum below.

3 Fits to $\eta' \to \pi^+\pi^-\gamma$ and $e^+e^- \to \pi^+\pi^-$

For the pion VFF, defined in Eq. (2.2), we employ a dispersive representation

$$F_\pi^V(s) = (1 + \alpha_\pi s)\Omega(s), \tag{3.1}$$

where

$$\Omega(s) = \exp\left\{ \frac{s}{\pi} \int_{4M_\pi^2}^\infty dx\, \frac{\delta_1^1(x)}{x(x - s - i\epsilon)} \right\} \tag{3.2}$$

is the Omnès function [82] and $\delta_1^1(s)$ denotes the $\pi\pi$ P-wave scattering phase shift in the isospin $I = 1$ channel. As input for the phase shift we use the solution of the Roy-equation analysis optimized for fits to pion VFF data of Ref. [27]. The term multiplying the Omnès function in Eq. (3.1) takes the effects of inelastic contributions, such as 4π, as well as our ignorance about the high-energy behavior of the phase shift into account, where the constant α_π is left as a free parameter to be constrained by the fit. The isospin-breaking effect of ρ–ω mixing in $e^+e^- \to \pi^+\pi^-$ is parameterized via

$$F_\pi^{V,e^+e^-}(s) = \left(1 + \epsilon_{\rho\omega} \frac{s}{M_\omega^2 - s - iM_\omega\Gamma_\omega}\right) F_\pi^V(s) \tag{3.3}$$

(in line with $\hat{t}_R(s)_{12}$ in Eq. (D.4)), where $\epsilon_{\rho\omega}$ will be determined by the fit.

In our formalism, the differential decay spectrum of $\eta' \to \pi^+\pi^-\gamma$ is described by [83]

$$\frac{d\Gamma(\eta' \to \pi^+\pi^-\gamma)}{ds} = 16\pi\alpha\Gamma_0 |F_\pi^V(s)|^2 \left| P(s) \right.$$
$$\left. + \frac{g_{\eta'\omega\gamma}\epsilon_{\rho\omega}}{g_{\omega\gamma}} \frac{1}{M_\omega^2 - s - iM_\omega\Gamma_\omega} \right|^2,$$
$$\Gamma_0 = \frac{2s}{3}\left(\frac{M_{\eta'}^2 - s}{16\pi M_{\eta'}}\sigma_\pi(s)\right)^3, \tag{3.4}$$

see Appendix D.2 for the derivation. The appearance of the pion VFF herein is due to the universality of $\pi\pi$ P-wave final-state interactions [76,84]. The constants A, β, and γ in $P(s)$, see Eq. (2.4), are used as fit parameters, and we refer to Eqs. (C.4) and (D.10) for the definitions of the coupling constants $g_{\omega\gamma}$ and $g_{\eta'\omega\gamma}$, respectively.

We fit to several time-like pion VFF data sets: provided by the $e^+e^- \to \pi^+\pi^-$ energy-scan experiments SND [85,86]

and CMD-2 [87–90], where in both cases diagonal errors were given, as well as from radiative-return measurements BaBar [91,92] (below 1 GeV) and KLOE [93–96], where in both cases statistical and systematic covariance matrices were provided. Furthermore, the recent data set for the $\eta' \to \pi^+\pi^-\gamma$ spectrum measured by BESIII [81] is used in the fit, which largely supersedes older data in statistical accuracy [97]. In order to avoid the d'Agostini bias [98] in the minimization of a χ^2 with naively constructed covariance matrices when dealing with normalization uncertainties, an iterative fit procedure, proposed in Ref. [99] and applied to $e^+e^- \to \pi^+\pi^-$ in Ref. [27], is employed. Since the pion VFF is defined as a pure QCD quantity in Eq. (2.2), the pion VFF data sets have been undressed of vacuum-polarization (VP) effects. As noted in Ref. [27], a minor rescaling of energy for each individual $\pi^+\pi^-$ data set leads to a significant improvement of the fit quality. Equivalently, we take the ω mass for individual data sets as a fit parameter. In the case of fitting the combined KLOE data set, we follow Ref. [27] and assign a global ω mass with individual mass shifts $\Delta M_\omega^{(i)}$ to each of the three underlying data sets, from 2008 [93], 2010 [94], and 2012 [95]. Furthermore, the mass shifts are constrained by penalties $\Delta\chi_i^2 = (\Delta M_\omega^{(i)}/\Delta E_c)^2$, with calibration uncertainty $\Delta E_c = 0.2$ MeV [100]. These terms are counted as additional data points in the number of degrees of freedom. Finally, for BaBar and KLOE the observables are cross sections weighted over energy bins, an effect that is also included in our fit in the same way as in Ref. [27]. Further data sets are available from BESIII [101] and SND [102], but not yet included for consistency: since we use the $\pi\pi$ phase shift from Ref. [27], we restrict our analysis to the same data sets used therein, in particular, since the results for the η' decays are insensitive to the precise choice of VFF data sets.

The BESIII data set for $\eta' \to \pi^+\pi^-\gamma$ includes the number of selected events, the number of background events, the detection efficiency, and the detector resolution root mean square in the respective energy bin. The latter is taken into account by taking the convolution of the theoretical spectrum in Eq. (3.4) with a Gaussian distribution of mean corresponding to the respective bin center and standard deviation given by the respective value for the energy resolution. Efficiency and number of background events are subsequently included in the fit function. Since the data are given in the form of an event rate, the physical values of the fit parameters A and $\epsilon_{\rho\omega}$ are extracted by utilizing the constraint

$$\Gamma(\eta' \to \pi^+\pi^-\gamma) = \int_{4M_\pi^2}^{M_{\eta'}^2} ds\, \frac{d\Gamma(\eta' \to \pi^+\pi^-\gamma)}{ds} \tag{3.5}$$

in the single fit to the BESIII decay spectrum, where the partial width $\Gamma(\eta' \to \pi^+\pi^-\gamma)$ is given by the corresponding quantities in Table 1. The couplings $g_{\omega\gamma}$ and $g_{\eta'\omega\gamma}$ have been

Table 1 Input parameters used in this work. Note that M_ω becomes a free parameter for the VFF fits, to account for the uncertainty in energy calibration in each data set as well as the tension with determinations from $e^+e^- \to 3\pi$ and $e^+e^- \to \pi^0\gamma$. The quoted numbers for M_ω, Γ_ω are VP subtracted, to ensure consistency with the bookkeeping as defined in the appendix. We also show the analog quantities for the ϕ, which enter the isoscalar part of the TFF (and are consistent with analogous determinations from $e^+e^- \to \bar{K}K$ [104]). The entries for $\Gamma(V \to e^+e^-)\text{Br}(V \to 3\pi)$, $V = \omega, \phi$, from Ref. [103] are consistent with but more precise than the current PDG averages

Quantity	Value	Reference
$M_{\eta'}$	957.78(6) MeV	[19]
$\Gamma_{\eta'}$	0.188(6) MeV	[19]
$F_{\eta'\gamma\gamma}$	0.3437(55) GeV^{-1}	[19]
Br($\eta' \to \pi^+\pi^-\gamma$)	29.5(4)%	[19]
M_ω	782.607(23) MeV	[31]
Γ_ω	8.69(4) MeV	[31]
$\Gamma(\omega \to e^+e^-)\text{Br}(\omega \to 3\pi)$	0.5698(31)(82) keV	[103]
Br($\omega \to 3\pi$)	89.2(7)%	[19]
Br($\eta' \to \omega\gamma$)	2.50(7)%	[19]
M_ϕ	1019.197(20) MeV	[31]
Γ_ϕ	4.22(5) MeV	[31]
$\Gamma(\phi \to e^+e^-)\text{Br}(\phi \to 3\pi)$	0.1841(21)(80) keV	[103]
Br($\phi \to 3\pi$)	15.24(33)%	[19]
Br($\phi \to \eta'\gamma$)	$6.22(21) \times 10^{-5}$	[19]

Table 2 Comparison of the fit outcome of the differential decay width in Eq. (3.4) to the BESIII $\eta' \to \pi^+\pi^-\gamma$ spectrum [81] of the binned maximum likelihood and minimum χ^2 strategies

Quantity	Likelihood	χ^2
A [GeV^{-3}]	17.10(35)	17.07(32)
β [GeV^{-2}]	0.589(53)	0.599(51)
γ [GeV^{-4}]	−0.204(53)	−0.214(50)
$\epsilon_{\rho\omega} \times 10^3$	1.624(73)	1.622(55)
M_ω [MeV]	783.07(33)	783.08(31)

where n_i represents the number of events in bin i and μ_i is the value of the fit function in this energy bin. This proves to be disadvantageous for our purpose, since we aim at a combined χ^2 fit of the pion VFF data sets and the $\eta' \to \pi^+\pi^-\gamma$ spectrum in order to extract a common ρ–ω mixing parameter $\epsilon_{\rho\omega}$. In Table 2, the fit parameters to the BESIII data stemming from the binned maximum likelihood method are compared to those of a χ^2 fit, by minimizing

$$\chi^2 = \sum_i \left(\frac{\mu_i - n_i}{\sigma_i} \right)^2, \tag{3.8}$$

where Poissonian errors $\sigma_i = \sqrt{n_i}$ have been assumed. The χ^2 fit gives a $\chi^2/\text{dof} = 1.78$ and the errors of the fit parameters have been inflated by a scale factor $\sqrt{\chi^2/\text{dof}}$. While the central values all agree with each other within error margins, the error estimates of the χ^2 fit are slightly lower than those of the binned maximum likelihood fit, but sufficiently close to justify a χ^2 fit in combination with VFF data. The quoted errors for the extracted values of A and $\epsilon_{\rho\omega}$ include the errors of all fit parameters and their correlations through Eq. (3.5) as well as the errors of the experimental input parameters.

In the combined fit of the $\eta' \to \pi^+\pi^-\gamma$ spectrum and the pion VFF data sets, the ρ–ω mixing parameter $\epsilon_{\rho\omega}$ is a shared parameter. In comparison to the $\eta' \to \pi^+\pi^-\gamma$ single fit, we are confronted with the problem that we fit the physical value of $\epsilon_{\rho\omega}$ and not the one including the event rate N_{ev}. Therefore, N_{ev} needs to be calculated at every step of the fit iteration. Defining $2P_{\text{ev}}(s) = N_{\text{ev}}A(1 + \beta s + \gamma s^2)$, Eq. (3.5) can be written as

$$0 = \mathcal{A}_2 N_{\text{ev}}^2 + \mathcal{A}_1 N_{\text{ev}} + \mathcal{A}_0, \tag{3.9}$$

where

$$\mathcal{A}_2 = -\Gamma(\eta' \to \pi^+\pi^-\gamma) + 16\pi\alpha \int_{4M_\pi^2}^{M_{\eta'}^2} \text{d}s \, \Gamma_0 |F_\pi^V(s)|^2$$

$$\times \frac{g_{\eta'\omega\gamma}^2 \epsilon_{\rho\omega}^2}{g_{\omega\gamma}^2} \frac{1}{(M_\omega^2 - s)^2 + M_\omega^2 \Gamma_\omega^2},$$
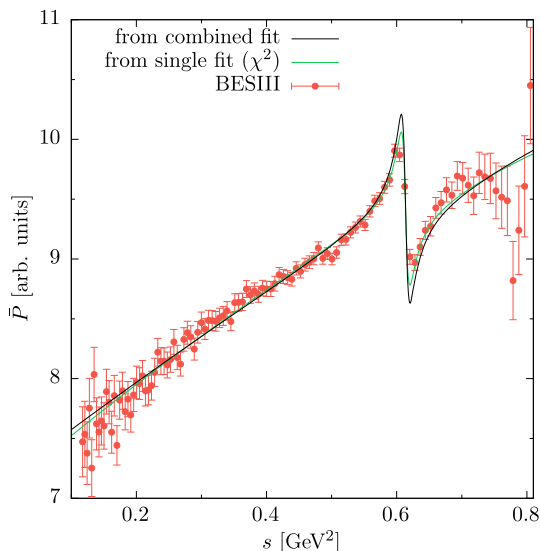
extracted by means of VMD models [83] to be

$$g_{\omega\gamma} = \sqrt{\frac{3\Gamma(\omega \to e^+e^-)}{4\pi\alpha^2 M_\omega}} = 0.0619(3),$$

$$g_{\eta'\omega\gamma} = -\sqrt{\frac{8M_{\eta'}^3 \Gamma(\eta' \to \omega\gamma)}{\alpha(M_{\eta'}^2 - M_\omega^2)^3}} = -0.400(8) \text{ GeV}^{-1}, \tag{3.6}$$

where the experimental input quantities are listed in Table 1 as well. Note that the definition of the coupling $g_{\eta'\omega\gamma}$ differs from the one in Ref. [83] by a factor of the elementary charge e, with such factors always factorized throughout this work. Also note that the given value for the coupling $g_{\omega\gamma}$ has been corrected for VP in order to be consistent with the definition of the pion VFF as a pure QCD quantity. The correction amounts to a factor of $|1 - \Pi(M_\omega^2)| = 0.977$, where $\Pi(s)$ is the Standard Model VP function of Ref. [26].

In principle, the provided data would need to be fit by the binned maximum likelihood strategy, i.e., by minimizing the log-likelihood function

$$\mathcal{L} = -\sum_i \log \left(\frac{(\mu_i)^{n_i} e^{-\mu_i}}{n_i!} \right), \tag{3.7}$$

Fig. 1 Fit to the differential decay rate of $\eta' \to \pi^+\pi^-\gamma$ (individually or combined with the VFF). To highlight differences in the ρ–ω region, we show the associated function $\bar{P}$, as defined in Eq. (3.11), compared to the experimental data from BESIII [81]. The function $\bar{P}$ is calculated in units that still contain the event rate

$$
\mathcal{A}_1 = 32\pi\alpha \int_{4M_\pi^2}^{M_{\eta'}^2} \mathrm{d}s \, \Gamma_0 |F_\pi^V(s)|^2 P_{\mathrm{ev}}(s) \frac{g_{\eta'\omega\gamma}\epsilon_{\rho\omega}}{g_{\omega\gamma}}
$$
$$
\times \frac{M_\omega^2 - s}{(M_\omega^2 - s)^2 + M_\omega^2 \Gamma_\omega^2},
$$
$$
\mathcal{A}_0 = 16\pi\alpha \int_{4M_\pi^2}^{M_{\eta'}^2} \mathrm{d}s \, \Gamma_0 |F_\pi^V(s)|^2 P_{\mathrm{ev}}^2(s), \tag{3.10}
$$

and notation as in Eq. (3.4), in order to determine N_{ev} with input of $\epsilon_{\rho\omega}$ in physical units. Hence, the main difference to the individual fit is that to be able to perform a combined fit with the VFF data sets, we need to ensure physical units already at each step in the fit iteration. The linear parameter α_π in the pion VFF is used as a shared parameter for all data sets in the combined fit as well.

The result of the combined fit is listed in Table 3, where the errors are inflated by the overall $\sqrt{\chi^2/\mathrm{dof}}$. The error of the physical value of A takes into account the correlations and inflated errors of the fit parameters as well as the errors of all input quantities. The results for M_ω and $\epsilon_{\rho\omega}$ are in good agreement with Ref. [27], validating the simplified fit form (3.1) as a convenient way to compare ρ–ω mixing in the pion VFF and $\eta' \to \pi^+\pi^-\gamma$. The outcome of the combined fit for the case of the $\eta' \to \pi^+\pi^-\gamma$ spectrum is shown in Fig. 1, where

$$
\bar{P}(s) = \left[\frac{1}{\Gamma_0 |\Omega(s)|^2} \frac{\mathrm{d}\Gamma(\eta' \to \pi^+\pi^-\gamma)}{\mathrm{d}s} \right]^{1/2} \tag{3.11}
$$

is shown to emphasize differences in the vicinity of the ρ–ω mixing effect.

Both in Fig. 1 and by comparing Tables 2 and 3, one sees that both processes are not fully consistent, with the tension in $\epsilon_{\rho\omega}$ the most apparent one: the $\eta' \to \pi^+\pi^-\gamma$ data prefer a value $\epsilon_{\rho\omega} \simeq 1.6(1) \times 10^{-3}$, while the combined fit, statistically dominated by the VFF data sets, produces a value close to $\epsilon_{\rho\omega} \simeq 2.0 \times 10^{-3}$, with negligible uncertainty at the level of the difference. This mismatch is highlighted by the presentation as in Fig. 1, and comes out substantially larger than any effect that could be obtained by variation of fit strategy and choice of input parameters. In none of the variants we studied did the combination of experimental errors and external input suggest an uncertainty beyond $\Delta\epsilon_{\rho\omega} \simeq 0.1 \times 10^{-3}$, which leads us to conclude that this tension is significant.

A minor tension also occurs in the mass of the ω.[1] Here, the results from 2π come out significantly below the preferred value from $e^+e^- \to 3\pi, \pi^0\gamma$ [28,31], see Table 1, but extractions from 2π are known to be sensitive to a phase in $\epsilon_{\rho\omega}$ [92], with the corresponding difference at least partially explained by radiative intermediate states that can generate such an isospin-breaking effect [105]. In contrast, the $\eta' \to \pi^+\pi^-\gamma$ data favor a central value that deviates about 0.5 MeV in the opposite direction, albeit with moderate significance. Since also the recent 3π data from BESIII [106] suggest a similar increase compared, e.g., to Refs. [88,103,107], as does Ref. [101] compared to other 2π data sets, it is difficult not to see a pattern in BESIII determinations of M_ω.

4 Predicting $\eta' \to \ell^+\ell^-\gamma$

In order to determine the η' TFF according to Eq. (2.3), the ρ–ω mixing parameter $\epsilon_{\rho\omega}$, the parameter associated with inelastic contributions to the pion VFF α_π, as well as the polynomial parameters A, β, and γ of the $\eta' \to \pi^+\pi^-\gamma$ spectrum from the combined fit serve as input. Additionally, from the quantities listed in Table 1, the ω mass and width, the TFF normalization $F_{\eta'\gamma\gamma}$, together with the associated couplings in Eq. (3.6) enter the description of the isovector part of the TFF. The isoscalar part, consisting of the contributions of the ω and ϕ resonances, depends on the couplings $w_{\eta'V\gamma}$ in Eq. (D.9), which were calculated from the quantities in Table 1. In the time-like regime, the resulting TFF then appears as shown in Fig. 2, where it is compared to experimental data [108].

---

[1] Note that constraining the relative shifts in the ω masses from the expected uncertainty in the energy calibration, in a similar fashion as it was done here in the combined fit for the case of KLOE, only leads to marginal changes in the results compared to the ones displayed in Table 3 for the other pion VFF data sets, see Ref. [27].

Table 3 Combined fit to several pion VFF data sets (BaBar, KLOE, CMD-2, SND) and $\eta' \to \pi^+\pi^-\gamma$ spectrum (BESIII) with overall $\chi^2/\text{dof} = 1.64$. In the row for KLOE, the three values for M_ω refer to the combinations of the global KLOE ω mass and the corresponding mass shifts of the three underlying data sets from 2008, 2010, 2012, respectively. See main text for details

	χ^2/dof	M_ω [MeV]	A [GeV^{-3}]	β [GeV^{-2}]	γ [GeV^{-4}]	$\alpha_\pi \times 10^2$ [GeV^{-2}]	$\epsilon_{\rho\omega} \times 10^3$
BaBar	1.27	781.780(88)					
KLOE	1.60	781.67(13)					
		782.11(18)				5.72(14)	1.994(11)
		781.86(28)					
CMD-2	2.17	782.139(73)					
SND	2.16	781.47(10)					
BESIII	2.36	783.12(27)	17.29(33)	0.523(46)	−0.138(46)		

Since the form of polynomial $P(s)$ and the linear polynomial multiplying the Omnès function in the representation of the pion VFF are governed by physics below 1 GeV, their values at high energies do not bear much meaning. Therefore, and in order to improve the convergence properties of the dispersion integrals in Eq. (2.3) at the same time, they are led to constant values $P(s_c)$ and $1 + \alpha_\pi s_c$ above a certain cutoff value s_c. This cutoff is varied between $s_c = 1 \text{ GeV}^2$, the point where $P(s)$ reaches its maximum ($s_c = 1.89 \text{ GeV}^2$ with β and γ from the combined fit) and the point where P drops below its value at $s = 0$ ($s_c = 3.79 \text{ GeV}^2$). Together with the errors of the input quantities in Table 1, the errors of the parameters from the combined fit, and their correlations, this procedure is used to generate the error band of the dispersive η' TFF representation shown in Fig. 2. In this figure, the dispersive curve displays the broad ρ peak from the isovector part of the TFF. Around the ω mass, the ρ–ω mixing effect is overlaid by the narrow peak of the ω resonance from the isoscalar part of the TFF. Slightly below an invariant mass square of 1 GeV^2 the isoscalar ϕ contribution begins to set in. The available experimental data are in excellent agreement with the dispersive prediction, but not accurate enough to distinguish it from the VMD model. Figure 2 also shows the peak of the ϕ resonance, which, however, is not accessible in η' decays, but could be scanned in $e^+e^- \to \eta'\gamma$ near threshold.

The low-energy properties of the TFF are described by the slope parameter $b_{\eta'}$, which is defined by

$$F_{\eta'\gamma^*\gamma^*}(s, 0) = F_{\eta'\gamma\gamma}\left(1 + b_{\eta'}s + \mathcal{O}(s^2)\right). \quad (4.1)$$

It can be calculated via a sum rule, following from Eq. (2.3), and disentangled into its isovector contribution

$$b_{\eta'}^{(I=1)} = \frac{1}{48\pi^2 F_{\eta'\gamma\gamma}} \int_{4M_\pi^2}^{\infty} \frac{dx}{x} \sigma^3(x) P(x)|F_\pi^V(x)|^2, \quad (4.2)$$

and isoscalar contribution

$$b_{\eta'}^{(I=0)} = \sum_{V \in \{\omega, \phi\}} \frac{w_{\eta'V\gamma}}{M_V^2}, \quad (4.3)$$

with $b_{\eta'} = b_{\eta'}^{(I=1)} + b_{\eta'}^{(I=0)}$. Numerical values are listed together with the evaluation of the sum rule for the normalization (D.21) in Table 4. As expected from VMD, the isovector part dominates both the normalization and the slope, saturating the former by 70% and producing about 80% of the latter. In combination with the isoscalar part the sum rule for the normalization is fulfilled by 95%, suggesting a slightly faster convergence than similar sum rules in Refs. [40,41,110,111]. The two isospin-breaking corrections to the normalization, in the isovector and isoscalar part, combine to about −0.3% and thus prove negligible compared to the uncertainty in the sum-rule evaluation. Accordingly, these corrections become most relevant in the resonance region, where even subleading effects are enhanced by the small width of the ω resonance, see Fig. 2. The ω resonance peak would be about 4% increased in magnitude if $\epsilon_{\rho\omega} = 0$.

Our result for the slope,

$$b_{\eta'} = 1.455(24) \text{ GeV}^{-2}, \quad (4.4)$$

is consistent with, but considerably more precise than the experimental determinations $b_{\eta'} = 1.60(17)(8) \text{ GeV}^{-2}$ [108] (from $\eta' \to e^+e^-\gamma$) and $b_{\eta'} = 1.60(16) \text{ GeV}^{-2}$ [112], $b_{\eta'} = 1.38(23) \text{ GeV}^{-2}$ [113] (via $e^+e^- \to e^+e^-\eta'$), and also agrees very well with $b_{\eta'} = 1.43(4)(1) \text{ GeV}^{-2}$ [16] extracted via Padé approximants. Moreover, the improved formalism and combined fit allowed us to substantially reduce the uncertainties compared to the previous dispersion-theoretical analysis $b_{\eta'} = 1.53^{+0.15}_{-0.08} \text{ GeV}^{-2}$ [77], also reflecting the improved input on $\eta' \to \pi^+\pi^-\gamma$ from Ref. [81] in comparison to the earlier measurement [97]. A close-up of the low-s region of the TFF is included in Fig. 2 as well.
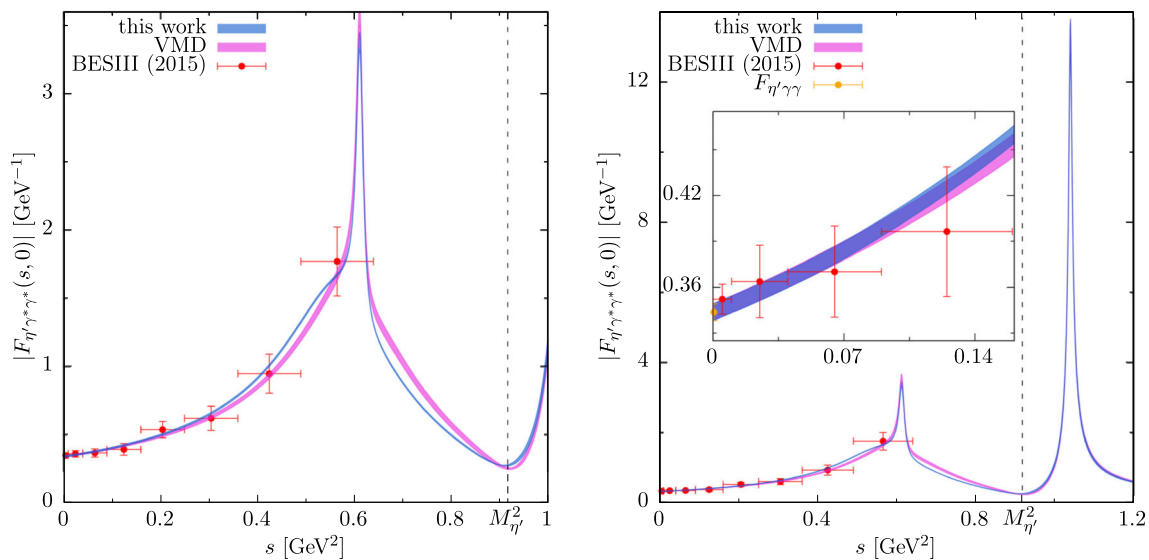
Fig. 2 Determination of the η' TFF by means of Eq. (2.3) in comparison to data from BESIII [108] (statistical and systematic errors added in quadrature) scaled with $F_{\eta'\gamma\gamma}$ from Table 1 and the VMD model of Eq. (D.23) with ϕ resonance contribution according to Eq. (D.22); for the kinematic range accessible in η' decays (left) and a larger time-like region including the ϕ resonance with inset magnifying the low-s region (right). See also Ref. [109] for an earlier version of this figure

Table 4 Contributions from the various components of the TFF to the sum rules of the normalization and the slope parameter

	$(I=1)_{\epsilon_{\rho\omega}=0}$	$\Delta(I=1)_{\epsilon_{\rho\omega}\neq 0}$	$(I=0)^{\omega}_{\epsilon_{\rho\omega}=0}$	$\Delta(I=0)^{\omega}_{\epsilon_{\rho\omega}\neq 0}$	$(I=0)^{\phi}$	Total
Norm [%]	71.85(93)	$-0.1433(20)$	7.20(23)	$-0.1389(46)$	15.85(61)	94.6(1.2)
$b_{\eta'}$ [GeV^{-2}]	1.185(23)	0	0.1176(32)	0	0.1526(53)	1.455(24)

5 Conclusions

This work presents progress in a dispersive calculation of the TFF of the η', as required for future studies of the η'-pole contribution to HLbL scattering in the anomalous magnetic moment of the muon. First, we established a formalism that enables a consistent implementation of isospin-breaking ρ–ω mixing effects, both in the isoscalar and isovector part of the form factor. The technical derivation is presented in a self-contained way in the appendices of the paper, leading to our main result (2.3) for the final TFF representation. Moreover, we worked out how the information on the isovector TFF contained in the spectrum for $\eta' \to \pi^+\pi^-\gamma$ can be combined, in terms of the decomposition (3.4).

These results form the basis for the application studied in the main part of the paper, an analysis of recent data from BESIII on $\eta' \to \pi^+\pi^-\gamma$ and subsequent prediction of the full η' TFF. A combined fit of the $\eta' \to \pi^+\pi^-\gamma$ spectrum and data on the pion VFF reveals a tension in the ρ–ω mixing parameter, with the former suggesting a substantially smaller value than extracted from isospin breaking in $e^+e^- \to \pi^+\pi^-$, see Fig. 1. Given the modest fit quality already in the individual fit as well as another minor tension in the ω mass, it would be desirable to scrutinize these observations with an independent measurement of the $\eta' \to \pi^+\pi^-\gamma$ spectrum, e.g., from CLAS at Jefferson Lab [114].

As a final step, we used the parameters determined in the global fit to $\eta' \to \pi^+\pi^-\gamma$ and $e^+e^- \to \pi^+\pi^-$, in combination with up-to-date input on the isoscalar resonances, to predict the full TFF at low energies, see Fig. 2 and Table 4. Deviations from VMD are most visible in the vicinity of the ω resonance, where the dispersive implementation of the ρ meson via 2π intermediate states changes the line shape compared to the strict VMD limit. Our results should prove valuable for the analysis of future data on $\eta' \to \pi^+\pi^-\gamma$ and $\eta' \to \ell^+\ell^-\gamma$ [115,116], in particular towards improving the calculation of the η'-pole contribution to HLbL scattering.

Appendix A: Coupled-channel formalism

In Appendix B–Appendix D, we derive a coupled-channel formalism for $\pi^+\pi^-$, $\ell^+\ell^-$, and $\pi^+\pi^-\pi^0$, concentrating on the ω resonance for the latter. In particular, we aim at delineating the impact of ρ–ω mixing on the pion vector form factor and pseudoscalar decays in a consistent way, leading to the master formulae with which the η' decays are analyzed in the main part. The construction follows the formalism developed in Ref. [80] (cf. also Refs. [117,118]), which can be summarized as follows: the full scattering amplitude $t(s)$, carrying channel indices i, j, is written as[2]

$$t(s)_{ij} = \tilde{t}(s)_{ij} + \xi_i \Gamma_{\mathrm{out}}(s)_i t_R(s)_{ij} \Gamma_{\mathrm{in}}(s)_j^\dagger \xi_j, \qquad (A.1)$$

where t_R denotes the part of the scattering amplitude that arises from iterating a resonance potential

$$t_R(s)_{ij} = \big[\mathbb{1} - V_R(s)\Sigma(s)\big]_{ik}^{-1} V_R(s)_{kj}, \qquad (A.2)$$

via the self energies

$$\Sigma(s)_{ij} = \delta_{ij} \frac{s}{\pi} \int_{s_{\mathrm{thr}}^i}^{\infty} \mathrm{d}s' \frac{\tilde{\sigma}_i(s')\xi_i^2 |\Gamma(s')_i|^2}{s'(s'-s-i\epsilon)}, \qquad (A.3)$$

with phase space $\tilde{\sigma}_i$, centrifugal barrier factors ξ_i, and vertex functions Γ_i. The potential is parameterized in terms of bare resonances

$$\bar{V}_R(s)_{ij} = -\sum_{l,l'=1}^{n} g_i^{(l)} G_{ll'} g_j^{(l')}, \qquad G_{ll'} = \frac{\delta_{ll'}}{s - m_l^2},$$
$$V_R(s) = \bar{V}_R(s) - \bar{V}_R(0), \qquad (A.4)$$

with bare masses m_l and then (potentially) subtracted at $s = 0$. For our application, this formalism is attractive, as it allows us to account for the physics of photon and ω exchange via V_R, the $\pi\pi$ rescattering via Omnès factors in the Γ_i, and combine everything in a way that is consistent with analyticity and unitarity. In addition, form factors (and thereby pseudoscalar decays) can be described in a similar way

$$F(s)_i = \Gamma_{\mathrm{out}}(s)_i \big[\mathbb{1} - V_R(s)\Sigma(s)\big]_{ik}^{-1} M_k, \qquad (A.5)$$

with source terms parameterized as

$$M_k = c_k - \sum_{l,l'=1}^{n} g_k^{(l)} G_{ll'} \alpha^{(l')} s, \qquad (A.6)$$

where the factor s in the resonance coupling arises as a consequence of gauge invariance. In the following, we will develop this formalism step by step for a three-channel system $\{2\pi, \ell^+\ell^-, 3\pi\}$, mediated via two resonances $\{\gamma, \omega\}$. Note that the ρ resonance is already contained in $\tilde{t}(s)$ for the 2π channel and thus also in the corresponding vertex function $\Gamma(s)$.

Appendix B: $\pi^+\pi^-$ and $\ell^+\ell^-$

Appendix B.1: $\pi\pi$ channel

As a first step we consider the single-channel case when only external $\pi^+\pi^-$ states and photon exchange are retained. The isospin $I = 1$ $\pi\pi$ scattering amplitude is written in the conventions

$$\mathcal{M}^1(s,t) = 32\pi \sum_{\mathrm{odd}\ l}(2l+1)t_l^1(s)P_l(z), \qquad (B.1)$$

with Legendre polynomials $P_l(z)$ and normalized in such a way that the cross section reads

$$\frac{\mathrm{d}\sigma}{\mathrm{d}\Omega} = \frac{|\mathcal{M}|^2}{64\pi^2 s}. \qquad (B.2)$$

The P-wave amplitude is identified with $\tilde{t}(s)$ in Eq. (A.1) as

$$\tilde{t}(s) \equiv 48\pi t_1^1(s) = \frac{e^{2i\delta_1^1(s)} - 1}{2i\tilde{\sigma}_\pi(s)},$$
$$\tilde{\sigma}_\pi(s) = \frac{\sigma_\pi(s)}{48\pi}, \quad \sigma_\pi(s) = \sqrt{1 - \frac{4M_\pi^2}{s}}. \qquad (B.3)$$

This definition is motivated by the isospin decomposition of the physical amplitude

$$\mathcal{M}^{\pi^+\pi^-} = \frac{1}{6}\mathcal{M}^2 - \frac{1}{2}\mathcal{M}^1 + \frac{1}{3}\mathcal{M}^0, \qquad (B.4)$$

since then $\mathcal{M}^{\pi^+\pi^-}|_{P\text{-wave}} = -t(s)z$ and $t(s)$ can essentially be interpreted as the standard amplitude with the angular dependence removed.

In addition, we can match the contribution from the s-channel photon-exchange diagram

$$\mathcal{M}_\gamma^{\pi^+\pi^-} = \frac{e^2}{s}\left(s - 4M_\pi^2\right)z\left(F_\pi^V(s)\right)^2 \tag{B.5}$$

to the second term in Eq. (A.1). That is, including the hadronic running of α for self consistency, we have

$$t_\gamma(s) = -\frac{4\pi\alpha}{s}\left(s - 4M_\pi^2\right)\left(F_\pi^V(s)\right)^2(1 - \Pi_\pi(s))^{-1},$$

$$\Pi_\pi(s) = -\frac{4\pi\alpha}{s}\frac{s^2}{\pi}\int_{4M_\pi^2}^\infty \mathrm{d}s'\frac{\tilde{\sigma}_\pi(s')(s' - 4M_\pi^2)|F_\pi^V(s')|^2}{s'^2(s' - s - i\epsilon)}, \tag{B.6}$$

which takes the form

$$t_\gamma(s) = \frac{V_R(s)\xi_\pi^2(s)\Gamma_{\text{out}}(s)\Gamma_{\text{in}}^\dagger(s)}{1 - V_R(s)\Sigma_\pi(s)}$$

$$= \xi_\pi^2(s)\Gamma_{\text{out}}(s)\Gamma_{\text{in}}^\dagger(s)t_R(s), \tag{B.7}$$

provided that we identify

$$\Gamma_{\text{out}}(s) = \Gamma_{\text{in}}^\dagger(s) = F_\pi^V(s), \qquad V_R(s) = -\frac{4\pi\alpha}{s},$$

$$\xi_\pi(s) = \sqrt{s - 4M_\pi^2},$$

$$\Sigma_\pi(s) = \frac{s^2}{\pi}\int_{4M_\pi^2}^\infty \mathrm{d}s'\frac{\tilde{\sigma}_\pi(s')\xi_\pi^2(s')|\Gamma(s')|^2}{s'^2(s' - s - i\epsilon)}. \tag{B.8}$$

The full result

$$t(s) = \tilde{t}(s) + \xi_\pi(s)\Gamma_{\text{out}}(s)t_R(s)\Gamma_{\text{in}}^\dagger(s)\xi_\pi(s) \tag{B.9}$$

then indeed agrees with Eq. (A.1), the only difference being that the self energy enters in twice-subtracted form.

Appendix B.2: $\ell^+\ell^-$ channel

In the leptonic channel we start from the VP function in the form

$$\Pi_\ell(s) = -\frac{4\pi\alpha}{s}\frac{s^2}{\pi}\int_{4m_\ell^2}^\infty \mathrm{d}s'\frac{\tilde{\sigma}_\ell(s')4(s' + 2m_\ell^2)}{s'^2(s' - s - i\epsilon)}, \tag{B.10}$$

which leads one to identify

$$\Gamma_{\text{out}}(s) = \Gamma_{\text{in}}(s) = 1, \quad V_R(s) = -\frac{4\pi\alpha}{s},$$

$$\xi_\ell(s) = 2\sqrt{s + 2m_\ell^2},$$

$$\Sigma_\ell(s) = \frac{s^2}{\pi}\int_{4m_\ell^2}^\infty \mathrm{d}s'\frac{\tilde{\sigma}_\ell(s')\xi_\ell^2(s')}{s'^2(s' - s - i\epsilon)}, \tag{B.11}$$

and thereby

$$t(s) = \xi_\ell^2(s)t_R(s) = \frac{\xi_\ell^2(s)V_R(s)}{1 - V_R(s)\Sigma_\ell(s)}. \tag{B.12}$$

This amplitude, when interpreted in the same way as the $\pi\pi$ amplitude $t(s)$ derived in the previous subsection, produces the total cross section[3]

$$\sigma(\ell^+\ell^- \to \ell^+\ell^-) = \frac{2\pi}{64\pi^2 s}\frac{1}{4}\left|\xi_\ell^2(s)V_R(s)\right|^2 \times \frac{2}{3}$$

$$= \frac{(4\pi\alpha)^2}{12\pi s^3}(s + 2m_\ell^2)^2, \tag{B.13}$$

which matches the QED result from the s-channel diagram (the factor $1/4$ averages over initial-state spins). In this way, the factor ξ_ℓ captures the kinematic dependence from the fermion traces instead of the centrifugal barrier, but up to this difference in interpretation the same decomposition applies as in the $\pi\pi$ channel.

Appendix B.3: Combining $\pi^+\pi^-$ and $\ell^+\ell^-$

The two-channel system $\{2\pi, \ell^+\ell^-\}$ with a photon mediator in $V_R(s)$ follows by combining the results from the previous two subsections:

$$t_R(s) = \left(\mathbb{1} - V_R(s)\Sigma(s)\right)^{-1}V_R(s), \tag{B.14}$$

$$V_R(s) = -\frac{4\pi\alpha}{s}\begin{pmatrix}1 & 1\\ 1 & 1\end{pmatrix}, \qquad \Sigma(s) = \text{diag}\left(\Sigma_\pi(s), \Sigma_\ell(s)\right),$$

so that

$$t_R(s) = -\frac{4\pi\alpha}{s}\begin{pmatrix}1 & 1\\ 1 & 1\end{pmatrix}\left(1 - \Pi(s)\right)^{-1},$$

$$\Pi(s) = -\frac{4\pi\alpha}{s}\left(\Sigma_\pi(s) + \Sigma_\ell(s)\right). \tag{B.15}$$

In particular, we find for the $e^+e^- \to \pi^+\pi^-$ cross section, by the same procedure as in Eq. (B.13),

$$\sigma(e^+e^- \to \pi^+\pi^-) = \frac{2\pi}{64\pi^2 s}\frac{1}{4}\frac{\sigma_\pi(s)}{\sigma_e(s)}\left|t(s)_{21}\right|^2 \times \frac{2}{3}$$

---

[3] The factor $2/3$ arises from the angular integral $\int_{-1}^1 \mathrm{d}z\,z^2$, as does represent the correct angular dependence for the bosonic amplitude in Eq. (B.5), but in general only the integrated quantities are reproduced correctly, since part of the angular dependence is moved into the centrifugal barrier factors, e.g., in contrast to ξ_π, the ξ_ℓ do not correspond to the center-of-mass momentum. Accordingly, we only keep the differential form when adequate, and otherwise simply display the integrated result.

$$= \frac{\pi \alpha^2}{3s} \frac{\sigma_\pi^3(s)|F_\pi^V(s)|^2}{|1 - \Pi(s)|^2} \frac{s + 2m_e^2}{s\sigma_e(s)},$$
(B.16)

which reproduces the expected result. Adding further leptonic channels is straightforward, e.g., in the VP function the sum of the lepton species appears. For simplicity, we will restrict the discussion to a single lepton channel throughout.

Appendix C: Including the 3π channel

Our main objective in including the 3π channel is as follows: since in the end we are mainly interested in the 2π channel, the impact of 3π states is only indirect, so that we do not aim at a full description of the $\gamma^* \to 3\pi$ amplitude as derived in Refs. [40,41,119], but at a consistent implementation of the ω, which, due to $\rho-\omega$ mixing, is how the 3π channel leaves its imprints in 2π. This motivates including the ω as a second mediator besides the photon in the resonance potential V_R.

Appendix C.1: 3π and $\ell^+\ell^-$

As a first step, we consider the $\ell^+\ell^-$ and 3π channels only, in order to fix the parameters in the potential. We make the ansatz

$$V_R(s) = -\frac{4\pi\alpha}{s} \begin{pmatrix} 1 & g_3 s \\ g_3 s & (g_3 s)^2 \end{pmatrix} - \frac{1}{s - M_{\omega,0}^2} \begin{pmatrix} 0 & 0 \\ 0 & g_{\omega 3}^2 \end{pmatrix},$$

$$\Sigma(s) = \mathrm{diag}\big(\Sigma_\ell(s), \Sigma_{3\pi}(s)\big),$$
(C.1)

with functions/couplings g_3, $g_{\omega 3}$, $\Sigma_{3\pi}(s)$, and bare ω mass $M_{\omega,0}$ to be determined in the following. The underlying idea is that the potential is generated by photon and ω states, where the ω is to be approximated by a narrow resonance, with parameters that correspond to renormalized versions of the bare parameters from Eq. (C.1).

In order to determine these parameters, we first consider the $\ell^+\ell^-$ component

$$t_R(s)_{22} = -\frac{4\pi\alpha}{s} \big(1 - \Pi_\ell(s) - \Pi_\omega(s)\big)^{-1},$$
(C.2)

where we have used the fact that VP is the only correction that should appear in $\ell^+\ell^-$ scattering. In a narrow-width approximation for the ω one would expect

$$\Pi_\omega(s) = \frac{e^2 g_{\omega\gamma}^2 s}{s - M_\omega^2 + iM_\omega\Gamma_\omega},$$
(C.3)

where the $\omega-\gamma$ coupling has been chosen in agreement with the Lagrangian definition

$$\mathcal{L}_{\omega\gamma} = -\frac{e}{2} g_{\omega\gamma} F^{\mu\nu} \omega_{\mu\nu}, \quad \omega_{\mu\nu} = \partial_\mu \omega_\nu - \partial_\nu \omega_\mu.$$
(C.4)

The potential in Eq. (C.1) produces

$$\Pi_\omega(s) = -e^2 s \big(s - M_{\omega,0}^2\big) \frac{g_3^2}{g_{\omega 3}^2}$$
$$+ \frac{e^2 s \big(\frac{g_3}{g_{\omega 3}}\big(s - M_{\omega,0}^2\big)\big)^2}{s - M_{\omega,0}^2 + \Sigma_{3\pi}(s) g_{\omega 3}^2},$$
(C.5)

demonstrating that g_3 in Eq. (C.1) indeed needs to be accompanied by a factor s to ensure gauge invariance. The comparison to Eq. (C.3) then suggests the identification[4]

$$\Sigma_{3\pi}(s) \equiv \Sigma_{3\pi} = \frac{M_{\omega,0}^2 - M_\omega^2 + iM_\omega\Gamma_\omega}{g_{\omega 3}^2},$$

$$g_{\omega\gamma} = -\frac{g_3}{g_{\omega 3}} \big(s - M_{\omega,0}^2\big).$$
(C.6)

The need to absorb an s dependence into $g_{\omega\gamma}$ shows that these relations are only strictly meaningful at the resonance mass, while polynomial ambiguities arise elsewhere. For the moment, we indicate this caveat by writing

$$\Pi_\omega(s) = P_\omega(s) + \frac{e^2 g_{\omega\gamma}^2 s}{s - M_\omega^2 + iM_\omega\Gamma_\omega},$$
(C.7)

with the role of the polynomial to be clarified in the following.

In total, the amplitudes in this two-channel system are

$$t_R(s)_{22} = -\frac{e^2}{s} \big(1 - \Pi(s)\big)^{-1},$$

$$t_R(s)_{23} = \frac{e^2 g_{\omega 3} g_{\omega\gamma}}{s - M_\omega^2 + iM_\omega\Gamma_\omega} \big(1 - \Pi(s)\big)^{-1},$$

$$t_R(s)_{33} = \left[\frac{\Pi_\omega(s)}{\Sigma_{3\pi}} - \frac{g_{\omega 3}^2 (1 - \Pi_\ell(s))}{s - M_\omega^2 + iM_\omega\Gamma_\omega} \right] \big(1 - \Pi(s)\big)^{-1},$$
(C.8)

where $\Pi(s) = \Pi_\ell(s) + \Pi_\omega(s)$.

Appendix C.2: Comparison to 2π and $\ell^+\ell^-$

The 2π channel could be treated in a similar way as 3π if the ρ were assumed to be narrow. In this case, one would write in the vicinity of the pole [120]

$$F_\pi^V(s) = \frac{g_{\rho\pi\pi} g_{\rho\gamma} s_\rho}{s_\rho - s},$$
(C.9)

[4] The sign in $g_{\omega\gamma}$ is motivated by the 2π channel and the definition of the $\rho-\omega$ mixing parameter, to match the sign conventions of Ref. [83].

with $g_{\rho\gamma}$ defined in analogy to $g_{\omega\gamma}$ and $g_{\rho\pi\pi}$ related to the decay width via

$$\Gamma_\rho = \frac{g_{\rho\pi\pi}^2 M_\rho}{48\pi} \sigma_\pi^3(M_\rho^2). \tag{C.10}$$

If we then assume the integral in Eq. (B.6) to be dominated by contributions close to the resonance and expand in Γ_ρ, we obtain

$$\Pi_\pi(s) = -\frac{e^2 g_{\rho\pi\pi}^2 g_{\rho\gamma}^2}{48\pi} \frac{M_\rho}{\Gamma_\rho} \sigma_\pi^3(M_\rho^2)$$
$$\times \frac{s}{\pi} \int_{4M_\pi^2}^{\infty} ds' \frac{\frac{M_\rho \Gamma_\rho}{(s'-M_\rho^2)^2+(M_\rho\Gamma_\rho)^2}}{s'-s-i\epsilon}. \tag{C.11}$$

The imaginary part of the integral can be read off from the $i\epsilon$ prescription, while in the narrow-width limit the numerator collapses to $\pi\delta(s'-M_\rho^2)$, producing

$$\Pi_\pi(s) = \frac{e^2 g_{\rho\gamma}^2 s}{s-M_\rho^2+iM_\rho\Gamma_\rho}, \tag{C.12}$$

which coincides with the narrow-width expectation for $\Pi_\omega(s)$ in Eq. (C.3). This indicates that ultimately the polynomial in Eq. (C.7) should be put to zero. In the same narrow-width approximation, the $e^+e^- \to \pi^+\pi^-$ peak cross section becomes

$$\sigma(e^+e^- \to \pi^+\pi^-)(M_\rho^2) = \frac{16\pi^2|\alpha(M_\rho^2)|^2 g_{\rho\gamma}^2}{M_\rho \sigma_e(M_\rho^2)}$$
$$\times \frac{\Gamma_\rho(M_\rho^2+2m_e^2)}{|s-M_\rho^2+iM_\rho\Gamma_\rho|^2}, \tag{C.13}$$

which can be used to interpret the result for the $e^+e^- \to 3\pi$ cross section (C.21) below.

Appendix C.3: $e^+e^- \to 3\pi$ cross section

To interpret results for the 3π channel we need to consider the cross section $e^+e^- \to 3\pi$. Its general form can be written as

$$\sigma(e^+e^- \to 3\pi)(s) = \int_{s_-}^{s_+} ds' \int_{t_-}^{t_+} dt' \frac{d^2\sigma(s',t';s)}{ds'\,dt'},$$
$$\frac{d^2\sigma(s',t';s)}{ds'\,dt'} = \frac{\alpha^2(s't'u'-M_\pi^2(s-M_\pi^2)^2)}{192\pi s^3}$$
$$\times |\mathcal{F}(s',t',u';s)|^2 \frac{s+2m_e^2}{s\sigma_e(s)}, \tag{C.14}$$

with $s'+t'+u' = s+3M_\pi^2$ and integration boundaries

$$s_- = 4M_\pi^2, \quad s_+ = (\sqrt{s}-M_\pi)^2,$$
$$t_\pm = \frac{1}{2}\big[s+3M_\pi^2-s' \pm \sigma_\pi(s')\lambda^{1/2}(s,M_\pi^2,s')\big]. \tag{C.15}$$

The scalar function $\mathcal{F}(s',t',u';s)$ is normalized as

$$\mathcal{F}(0,0,0;0) = F_{3\pi} = \frac{1}{4\pi^2 F_\pi^3}, \tag{C.16}$$

and decomposes as

$$\mathcal{F}(s',t',u';s) = a(s)f_{3\pi}(s',t',u'),$$
$$f_{3\pi}(s',t',u') = \Omega_1^1(s')+\Omega_1^1(t')+\Omega_1^1(u'), \tag{C.17}$$

as long as rescattering effects are neglected [121]. The simplest form of the normalization function consistent with Eq. (C.16) and including the ω resonance reads

$$a(s) = \frac{F_{3\pi}}{3}\left(1-c_{3\pi}\frac{s}{s-M_\omega^2+iM_\omega\Gamma_\omega}\right), \tag{C.18}$$

where VMD predicts $c_{3\pi} = 1$. A similar form holds for the 3π decay width:

$$\Gamma_\omega = \frac{1}{128(2\pi)^3 M_\omega^3} \int_{s_-}^{s_+} ds' \int_{t_-}^{t_+} dt'$$
$$\times \left(s't'u'-M_\pi^2(M_\omega^2-M_\pi^2)^2\right)|c_\omega|^2 |f_{3\pi}(s',t',u')|^2, \tag{C.19}$$

where we have written the normalization in terms of another constant c_ω, but assumed the same dependence on the Mandelstam variables as in Eq. (C.17). Numerically, this gives

$$\Gamma_\omega \approx 2.865 \times 10^{-7}\,\text{GeV}^7 |c_\omega|^2. \tag{C.20}$$

The peak cross section can then be expressed as

$$\sigma(e^+e^- \to 3\pi)(M_\omega^2) = \frac{16\pi^2\alpha^2 F_{3\pi}^2 |c_{3\pi}|^2}{9|c_\omega|^2 M_\omega \sigma_e(M_\omega^2)}$$
$$\times \frac{\Gamma_\omega(M_\omega^2+2m_e^2)}{|s-M_\omega^2+iM_\omega\Gamma_\omega|^2}. \tag{C.21}$$

Matching to the expected form (C.13) gives

$$|c_{3\pi}| = \frac{3|c_\omega|g_{\omega\gamma}}{F_{3\pi}} \approx 0.98, \tag{C.22}$$

demonstrating that, phenomenologically, $c_{3\pi}$ indeed comes out close to the VMD expectation. Finally, we remark that the form of the cross section (C.21) indeed matches onto

$|t_R(s)_{23}|^2$ from Eq. (C.8) as long as $\Gamma_\omega \propto |g_{\omega 3}|^2$, which clarifies the role of this parameter. To work out the explicit relation one would need to assign ξ_i and Γ_i for $i = 3\pi$, but since we will not consider 3π final states in the following, we do not pursue this avenue any further.

Appendix C.4: Pseudoscalar decays

In the formalism developed so far, the pseudoscalar decays of $P = \pi^0, \eta, \eta'$ into $\pi^+\pi^-\gamma$, $\ell^+\ell^-\gamma$, or $3\pi\gamma$ can be derived from Eq. (A.5), with a suitable choice of source terms M_k. To avoid the complications from ρ–ω mixing, we first consider the two-channel case $\{\ell^+\ell^-, 3\pi\}$, before generalizing to the full system in Appendix D.

For the 3π channel, the ansatz (A.6) applies, i.e., we can write

$$M_3 = a + \frac{g_{\omega 3}}{s - M_{\omega,0}^2}b + g_3 e^2 c, \tag{C.23}$$

with constants a, b, c to be determined in the following. Accordingly, to ensure consistency with Eq. (C.1), we have

$$M_2 = c\frac{e^2}{s}. \tag{C.24}$$

Using Eq. (A.2), we find

$$F_i(s) = \big(\Gamma_{\text{out}}(s)\big)_i \big(\mathbb{1} + t_R(s)\,\Sigma(s)\big)_{ij} M_j(s), \tag{C.25}$$

in particular,

$$F_2(s) = \frac{1}{1 - \Pi(s)}\left(\frac{e^2}{s}c + \frac{\Pi_\omega(s)}{s g_3}\left(a + \frac{g_{\omega 3}}{s - M_{\omega,0}^2}b\right)\right). \tag{C.26}$$

To interpret this form factor in the context of $P \to \ell^+\ell^-\gamma$ decays, we first consider the analog of Eq. (B.16) for a coupled-channel system of $\{\ell^+\ell^-, P\gamma\}$

$$\sigma(\ell^+\ell^- \to P\gamma) = \frac{2\pi}{64\pi^2 s}\frac{1}{4}\frac{\sigma_{P\gamma}(s)}{\sigma_\ell(s)}|t(s)_{24}|^2 \times \frac{2}{3}$$

$$\equiv \frac{\pi^2\alpha^3}{6s}\frac{\sigma_{P\gamma}^3(s)|F_{P\gamma^*\gamma^*}(s,0)|^2}{|1 - \Pi(s)|^2}\frac{\xi_\ell^2(s)}{\sigma_\ell(s)}, \tag{C.27}$$

where we defined the phase-space factor $\sigma_{P\gamma}(s) = (s - M_P^2)/s$. In addition, $V_R(s)$ is the same as in Eq. (B.14) and $\Gamma_{\text{out}}(s)_{P\gamma} = eF_{P\gamma^*\gamma^*}(s,0)$, leaving only $\xi_{P\gamma}(s)$ to be determined. The matching in Eq. (C.27) yields

$$\xi_{P\gamma}^2(s) = \frac{1}{2}\big(s - M_P^2\big)^2. \tag{C.28}$$

The same relation can also be derived from the $P\gamma$ contribution to the VP function $\Pi(s)$, supporting this assignment for a $P\gamma$ state, in terms of which the differential decay width becomes

$$\frac{\mathrm{d}\Gamma(P \to \ell^+\ell^-\gamma)}{\mathrm{d}s} = \frac{\alpha^3(M_P^2 - s)\xi_\ell^2(s)\xi_{P\gamma}^2(s)\sigma_\ell(s)}{12M_P^3 s^2}$$

$$\times \big|F_{P\gamma^*\gamma^*}(s,0)\big|^2. \tag{C.29}$$

Due to the final-state photon also the three-particle phase space can be simplified, producing

$$\frac{\mathrm{d}\Gamma(P \to \ell^+\ell^-\gamma)}{\mathrm{d}s} = \frac{1}{(2\pi)^3 32M_P^3}\big(M_P^2 - s\big)\sigma_\ell(s)\frac{1}{2}$$

$$\times \big|\mathcal{M}_{P \to \ell^+\ell^-\gamma}(s)\big|^2 \times \frac{2}{3}, \tag{C.30}$$

where we have written the general relativistic amplitude as $\mathcal{M}_{P \to \ell^+\ell^-\gamma}(s)$ in analogy to the scattering reactions studied before. The matching of Eqs. (C.29) and (C.30) then determines

$$\mathcal{M}_{P \to \ell^+\ell^-\gamma}(s) = \frac{e^2}{s}\xi_\ell(s)\xi_{P\gamma}(s)eF_{P\gamma^*\gamma^*}(s,0)$$

$$\equiv \xi_\ell(s)\xi_{P\gamma}(s)eF_2(s), \tag{C.31}$$

where the last step gives the identification with the outcome of our coupled-channel formalism. The parameter $c = F_{P\gamma\gamma}$ thus determines the TFF normalization, and defining, in analogy to Eq. (C.6), $\tilde{a} = -(s - M_{\omega,0}^2)a/g_{\omega 3}$, we find the relation

$$F_{P\gamma^*\gamma^*}(s,0) = F_{P\gamma\gamma} + \Pi_\omega(s)\frac{\tilde{a} - b}{g_{\omega\gamma}e^2}. \tag{C.32}$$

This again strongly suggests to set $P_\omega(s) = 0$ in Eq. (C.7), because then the matching

$$\tilde{a} - b \equiv -\frac{c_{3\pi}}{g_{\omega\gamma}}F_{P\gamma\gamma} \tag{C.33}$$

reproduces precisely the expected momentum dependence (C.18). Our final result for the $P \to \ell^+\ell^-\gamma$ amplitude, related to the decay width by Eq. (C.30), reads

$$\mathcal{M}_{P \to \ell^+\ell^-\gamma}(s) = \frac{\xi_\ell(s)\xi_{P\gamma}(s)}{1 - \Pi(s)}\frac{e^3 F_{P\gamma\gamma}}{s}$$

$$\times \left(1 - c_{3\pi}\frac{s}{s - M_\omega^2 + iM_\omega\Gamma_\omega}\right). \tag{C.34}$$

Appendix C.5: Radiative corrections to the ω pole parameters

As final step before generalizing to the full system we consider the modifications to the ω parameters when including VP corrections. Such modifications arise because of

$$1 - \Pi_\ell(s) - \Pi_\omega(s) = \left[s - M_\omega^2 + i M_\omega \Gamma_\omega - \frac{e^2 g_{\omega\gamma}^2 s}{1 - \Pi_\ell(s)} \right]$$
$$\times \frac{1 - \Pi_\ell(s)}{s - M_\omega^2 + i M_\omega \Gamma_\omega}. \quad \text{(C.35)}$$

Expanding the first factor in e,

$$s - M_\omega^2 + i M_\omega \Gamma_\omega - \frac{e^2 g_{\omega\gamma}^2 s}{1 - \Pi_\ell(s)}$$
$$= s\left(1 - e^2 g_{\omega\gamma}^2\right) - M_\omega^2 + i M_\omega \Gamma_\omega + \mathcal{O}\left(e^4\right)$$
$$\equiv \left(1 - e^2 g_{\omega\gamma}^2\right)\left(s - \bar{M}_\omega^2 + i \bar{M}_\omega \bar{\Gamma}_\omega\right) + \mathcal{O}\left(e^4\right), \quad \text{(C.36)}$$

we find that the new ω parameters are given by

$$\bar{M}_\omega = \left(1 + \frac{e^2 g_{\omega\gamma}^2}{2}\right) M_\omega + \mathcal{O}(e^4),$$
$$\bar{\Gamma}_\omega = \left(1 + \frac{e^2 g_{\omega\gamma}^2}{2}\right) \Gamma_\omega + \mathcal{O}(e^4), \quad \text{(C.37)}$$

and the couplings are renormalized according to

$$\bar{g}_{\omega3} = g_{\omega3}\sqrt{Z}, \quad \bar{g}_{\omega\gamma} = g_{\omega\gamma}\sqrt{Z}, \quad Z = 1 + e^2 g_{\omega\gamma}^2. \quad \text{(C.38)}$$

Numerically, these shifts are rather small, with $Z - 1 = 3.3 \times 10^{-4}$, i.e., the change in $g_{\omega\gamma}$ is completely negligible. As concerns the pole parameters [28,31],

$$\Delta M_\omega = \bar{M}_\omega - M_\omega = 0.13 \, \text{MeV},$$
$$\Delta \Gamma_\omega = \bar{\Gamma}_\omega - \Gamma_\omega = 1.4 \, \text{keV}, \quad \text{(C.39)}$$

the shift in the mass is comparable to current experimental uncertainties, while the main effect in the width comes instead from the interaction with the 2π channel. Using the approximation (C.12), one finds

$$\Delta \Gamma_\omega = \frac{e^2 g_{\omega\gamma}^2}{2} \Gamma_\omega + \frac{M_\omega^2}{\Gamma_\rho - \Gamma_\omega} e^2 g_{\rho\gamma}^2 \left(e^2 g_{\omega\gamma}^2 - 2\epsilon_{\rho\omega}\right)$$
$$= -0.06 \, \text{MeV}. \quad \text{(C.40)}$$

Appendix D: Full system

In this section, we present our final results for the full system $\{2\pi, \ell^+\ell^-, 3\pi\}$ with γ and ω mediators in the reso-

nance potential. We write the expressions in terms of the VP-subtracted ω parameters M_ω, Γ_ω, with the understanding that they are related to the physical pole parameters including VP by means of Eqs. (C.39) and (C.40). This convention simplifies expressions, and at the same time makes the factorization of VP manifest. We show the results for a single lepton species ℓ, with straightforward generalization to multiple generations.

Appendix D.1: Scattering channels

The ansatz for the full potential reads

$$V_R(s) = -\frac{4\pi\alpha}{s} \begin{pmatrix} 1 & 1 & g_3 s \\ 1 & 1 & g_3 s \\ g_3 s & g_3 s & (g_3 s)^2 \end{pmatrix}$$
$$- \frac{1}{s - M_{\omega,0}^2} \begin{pmatrix} g_{\omega2}^2 & 0 & g_{\omega2} g_{\omega3} \\ 0 & 0 & 0 \\ g_{\omega2} g_{\omega3} & 0 & g_{\omega3}^2 \end{pmatrix},$$
$$\Sigma(s) = \text{diag}\left(\Sigma_\pi(s), \Sigma_\ell(s), \Sigma_{3\pi}(s)\right), \quad \text{(D.1)}$$

where $g_{\omega2}$ parameterizes the isospin-breaking coupling of the 2π channel to the ω. In practice, we will neglect higher orders in $g_{\omega2}$, given that at this level also other subleading effects, such as the $\omega \to \pi^0\gamma$ channel, would need to be considered. The full VP function becomes

$$\Pi(s) = \Pi_\ell(s) + \Pi_\pi(s)\left(1 + \frac{2s\epsilon_{\rho\omega}}{M_\omega^2 - s - i M_\omega \Gamma_\omega}\right)$$
$$+ \Pi_\omega(s) + \mathcal{O}\left(g_{\omega2}^2\right), \quad \text{(D.2)}$$

with $\Pi_\omega(s)$ as defined in Eq. (C.3), and the ρ–ω mixing parameter

$$\epsilon_{\rho\omega} = g_{\omega2} g_{\omega\gamma}. \quad \text{(D.3)}$$

The full amplitudes are

$$t_R(s) = \frac{1}{1 - \Pi(s)} \hat{t}_R(s) + \mathcal{O}\left(g_{\omega2}^2\right),$$
$$\hat{t}_R(s)_{11} = -\frac{e^2}{s}\left(1 + \frac{2\epsilon_{\rho\omega}s}{M_\omega^2 - s - i M_\omega \Gamma_\omega}\right)$$
$$+ \frac{\epsilon_{\rho\omega}^2}{g_{\omega\gamma}^2} \frac{1}{M_\omega^2 - s - i M_\omega \Gamma_\omega},$$
$$\hat{t}_R(s)_{12} = -\frac{e^2}{s}\left(1 + \frac{\epsilon_{\rho\omega}s}{M_\omega^2 - s - i M_\omega \Gamma_\omega}\right),$$
$$\hat{t}_R(s)_{22} = -\frac{e^2}{s},$$
$$\hat{t}_R(s)_{13} = \frac{e^2 g_{\omega3} g_{\omega\gamma}}{s - M_\omega^2 + i M_\omega \Gamma_\omega}\left(1 - \frac{\epsilon_{\rho\omega}(1 - \Pi_\ell(s))}{e^2 g_{\omega\gamma}^2}\right),$$

$$\hat{t}_R(s)_{23} = \frac{e^2 g_{\omega 3} g_{\omega \gamma}}{s - M_\omega^2 + i M_\omega \Gamma_\omega} \left(1 - \frac{\epsilon_{\rho \omega} \Pi_\pi(s)}{e^2 g_{\omega \gamma}^2} \right),$$

$$\hat{t}_R(s)_{33} = \frac{\Pi_\omega(s)}{\Sigma_{3\pi}} \left(1 - \frac{2 \epsilon_{\rho \omega} \Pi_\pi(s)}{e^2 g_{\omega \gamma}^2} \right)$$

$$- \frac{g_{\omega 3}^2 (1 - \Pi_\ell(s) - \Pi_\pi(s))}{s - M_\omega^2 + i M_\omega \Gamma_\omega}. \qquad (D.4)$$

$t_R(s)_{23}$ and $t_R(s)_{33}$ indeed generalize Eq. (C.8), and in the conventions (C.6) the sign in the ρ–ω-mixing correction in $e^+ e^- \to \pi^+ \pi^-$ agrees with Ref. [83]. Note that the expansion in $g_{\omega 2}$ is clearly not appropriate for the isospin-violating corrections to $\pi^+ \pi^-$ scattering, where terms of order $\mathcal{O}(g_{\omega 2}^2)$ should be counted at the same order as $\mathcal{O}(e^2 g_{\omega 2})$. For completeness, we have therefore retained the corresponding correction in $t_R(s)_{11}$.

Appendix D.2: Decays and transition form factors

Generalizing Eqs. (C.23) and (C.24), we make the following ansatz for the source terms

$$M(s) = c \frac{e^2}{s} \begin{pmatrix} 1 \\ 1 \\ g_3 s \end{pmatrix} + \frac{b}{s - M_{\omega,0}^2} \begin{pmatrix} g_{\omega 2} \\ 0 \\ g_{\omega 3} \end{pmatrix} + \begin{pmatrix} -P(s) \\ 0 \\ a \end{pmatrix}, \qquad (D.5)$$

with parameters a, b, c to be interpreted as before, and only the role of the function $P(s)$ to be clarified. As a first step, the result for the $P \to \ell^+ \ell^- \gamma$ amplitude generalizes to

$$\mathcal{M}_{P \to \ell^+ \ell^- \gamma}(s) = \frac{\xi_\ell(s) \xi_{P\gamma}(s)}{1 - \Pi(s)} \frac{e^3}{s} F_{P\gamma^* \gamma^*}(s, 0),$$

$$F_{P\gamma^* \gamma^*}(s, 0) = F_{P\gamma\gamma} + P(s) \Sigma_\pi(s)$$

$$\times \left(1 + \frac{\epsilon_{\rho \omega} s}{M_\omega^2 - s - i M_\omega \Gamma_\omega} \right)$$

$$+ \frac{F_{P\gamma\gamma} w_{P\omega\gamma} s}{M_\omega^2 - s - i M_\omega \Gamma_\omega} \left(1 + \frac{\epsilon_{\rho \omega}}{s g_{\omega \gamma}^2} \Sigma_\pi(s) \right)$$

$$+ \mathcal{O}(e^2 \epsilon_{\rho \omega}). \qquad (D.6)$$

Here, we have eliminated the parameter $c_{3\pi}$ in favor of the ω contribution to the slope of the TFF[5]

$$c_{3\pi} \to M_\omega^2 b_P^\omega = \frac{M_\omega^2}{F_{P\gamma\gamma}} \frac{dF_{P\gamma^* \gamma^*}^\omega(s, 0)}{ds} \bigg|_{s=0} = w_{P\omega\gamma}, \qquad (D.7)$$

---

[5] For simplicity, we only consider $P = \eta, \eta'$, otherwise, the different isospin structure for the π^0 TFF would need to be taken into account. In particular, Eq. (D.8) produces $w_{\pi^0 \omega \gamma} \approx 0.5$, consistent with $c_{3\pi} = 2 w_{\pi^0 \omega \gamma}$ in this case.

where the weights are given by [18]

$$w_{PV\gamma}^2 = \begin{cases} \frac{9 M_V^2 M_P^3 \Gamma(V \to e^+ e^-) \Gamma(V \to P\gamma)}{2\alpha (M_V^2 - M_P^2)^3 \Gamma(P \to \gamma\gamma)} & \text{if } M_V > M_P, \\ \frac{3 M_P^6 \Gamma(V \to e^+ e^-) \Gamma(P \to V\gamma)}{2\alpha M_V (M_P^2 - M_V^2)^3 \Gamma(P \to \gamma\gamma)} & \text{if } M_P > M_V. \end{cases} \qquad (D.8)$$

Determining the signs by the comparison to VMD [18], the numerical values based on Table 1 are

$$w_{\eta' \omega \gamma} = 0.072(2), \quad w_{\eta' \phi \gamma} = 0.158(6), \qquad (D.9)$$

and in terms of couplings $g_{PV\gamma}$,

$$g_{PV\gamma}^2 = \begin{cases} \frac{24 \Gamma(V \to P\gamma)}{\alpha} \left(\frac{M_V}{M_V^2 - M_P^2} \right)^3 & \text{if } M_V > M_P, \\ \frac{8 \Gamma(P \to V\gamma)}{\alpha} \left(\frac{M_P}{M_P^2 - M_V^2} \right)^3 & \text{if } M_P > M_V, \end{cases} \qquad (D.10)$$

one finds

$$w_{PV\gamma}^2 = \frac{g_{PV\gamma}^2 g_{V\gamma}^2}{F_{P\gamma\gamma}^2}. \qquad (D.11)$$

In analogy to Eq. (C.30), we have

$$\frac{d\Gamma(P \to \pi^+ \pi^- \gamma)}{ds} = \frac{1}{(2\pi)^3 32 M_P^3} (M_P^2 - s) \sigma_\pi(s) \frac{1}{2}$$

$$\times |\mathcal{M}_{P \to \pi^+ \pi^- \gamma}(s)|^2 \times \frac{2}{3}, \qquad (D.12)$$

with

$$\mathcal{M}_{P \to \pi^+ \pi^- \gamma}(s) = -\frac{e F_\pi^V(s) \xi_\pi(s) \xi_{P\gamma}(s)}{1 - \Pi(s)} \left(P(s) + \mathcal{O}(e^2) \right.$$

$$\left. + \frac{F_{P\gamma\gamma} w_{P\omega\gamma} \epsilon_{\rho\omega}}{g_{\omega\gamma}^2} \frac{1}{M_\omega^2 - s - i M_\omega \Gamma_\omega} \right), \qquad (D.13)$$

where we have neglected non-resonant corrections $\mathcal{O}(e^2)$ in the isospin-conserving part and the coefficient of the ω admixture can be written as $g_{P\omega\gamma} \epsilon_{\rho\omega} / g_{\omega\gamma}$ due to Eq. (D.11). The resulting spectrum becomes

$$\frac{d\Gamma(P \to \pi^+ \pi^- \gamma)}{ds} = 16\pi \alpha \Gamma_0 |F_\pi^V(s)|^2 \bigg| P(s)$$

$$+ \frac{g_{P\omega\gamma} \epsilon_{\rho\omega}}{g_{\omega\gamma}} \frac{1}{M_\omega^2 - s - i M_\omega \Gamma_\omega} \bigg|^2,$$

$$\Gamma_0 = \frac{2s}{3} \left(\frac{M_P^2 - s}{16\pi M_P} \sigma_\pi(s) \right)^3 \qquad (D.14)$$

as given in Eq. (3.4), in agreement with Refs. [78,83] upon the identification $2P(s) = A(1 + \beta s + \gamma s^2)$ (and separating

the factor $e^2 = 4\pi\alpha$). The function $P(s)$ thus emerges as a parameterization of the $P \to \pi^+\pi^-\gamma$ spectrum.

Appendix D.3: Dispersion relations

The previous discussion now allows us to write down dispersion relations for the pseudoscalar TFF including a consistent treatment of ρ–ω mixing. Reading off the discontinuities from Eq. (D.6),

$$
\begin{aligned}
\mathrm{Im}_{\pi\pi}\, F_{P\gamma^*\gamma^*}(s,0) &= \frac{s}{48\pi}\sigma_\pi^3(s)|F_\pi^V(s)|^2 \Bigg[P(s) \\
&\times \left(1 + \frac{s\epsilon_{\rho\omega}}{M_\omega^2 - s - iM_\omega\Gamma_\omega}\right)^* \\
&+ \frac{F_{P\gamma\gamma}\,w_{P\omega\gamma}\,\epsilon_{\rho\omega}}{g_{\omega\gamma}^2}\frac{1}{M_\omega^2 - s - iM_\omega\Gamma_\omega}\Bigg],
\end{aligned}
$$

$$
\begin{aligned}
\mathrm{Im}_{3\pi}\, F_{P\gamma^*\gamma^*}(s,0) &= \pi s\,\delta(s - M_\omega^2)\Bigg[F_{P\gamma\gamma}\,w_{P\omega\gamma} \\
&\times \left(1 + \frac{\epsilon_{\rho\omega}}{g_{\omega\gamma}^2 s}\Sigma_\pi(s)\right)^* \\
&+ \epsilon_{\rho\omega}P(s)\Sigma_\pi(s)\Bigg],
\end{aligned} \tag{D.15}
$$

we first observe that, as expected, the sum of the double discontinuities vanishes:

$$
\begin{aligned}
\mathrm{Im}\left[\mathrm{Im}_{\pi\pi}\, F_{P\gamma^*\gamma^*}(s,0)\right] &= -\mathrm{Im}\left[\mathrm{Im}_{3\pi}\, F_{P\gamma^*\gamma^*}(s,0)\right] \\
&= \frac{s\epsilon_{\rho\omega}}{48}\sigma_\pi^3(s)|F_\pi^V(s)|^2\delta(s - M_\omega^2) \\
&\times \left(\frac{F_{P\gamma\gamma}\,w_{P\omega\gamma}}{g_{\omega\gamma}^2} - sP(s)\right).
\end{aligned} \tag{D.16}
$$

Next, we replace

$$
P(s)\Sigma_\pi(s) \to \frac{s}{48\pi^2}\int_{4M_\pi^2}^\infty \mathrm{d}s'\frac{\sigma_\pi^3(s')P(s')|F_\pi^V(s')|^2}{s' - s - i\epsilon}, \tag{D.17}
$$

which does not affect the cancellation of the double discontinuities, but ensures that all dispersive integrals related to $\Sigma_\pi(s)$ have the same convergence properties. In the end, this step amounts to a choice of subtraction scheme, which, in the coupled-channel formalism, corresponds to polynomial ambiguities.

To derive a dispersive representation for the TFF, we start from the once-subtracted version

$$
\begin{aligned}
F_{P\gamma^*\gamma^*}(s,0) &= F_{P\gamma\gamma} + \frac{s}{\pi}\int_{4M_\pi^2}^\infty \mathrm{d}s' \\
&\times \frac{\sum_{i=\pi\pi,3\pi} \mathrm{Im}_i F_{P\gamma^*\gamma^*}(s',0)}{s'(s'-s)}.
\end{aligned} \tag{D.18}
$$

To keep track of the ω propagator consistently at all stages of the calculation, it is useful to replace

$$
\frac{s}{M_\omega^2 - s - iM_\omega\Gamma_\omega} \to \frac{s}{\pi}\int \mathrm{d}s'\frac{\pi\delta(s' - M_\omega^2)}{s' - s - i\epsilon} \tag{D.19}
$$

and only restore the finite width in the end.[6] Combining denominators in the various dispersion integrals, one can show that indeed the ω propagator factorizes, leading to a form very similar to Eq. (D.6):

$$
\begin{aligned}
F_{P\gamma^*\gamma^*}(s,0) &= F_{P\gamma\gamma} + \left[1 + \frac{\epsilon_{\rho\omega}s}{M_\omega^2 - s - iM_\omega\Gamma_\omega}\right] \\
&\times \frac{s}{48\pi^2}\int_{4M_\pi^2}^\infty \mathrm{d}s'\frac{\sigma_\pi^3(s')P(s')|F_\pi^V(s')|^2}{s' - s - i\epsilon} \\
&+ \frac{F_{P\gamma\gamma}\,w_{P\omega\gamma}\,s}{M_\omega^2 - s - iM_\omega\Gamma_\omega}\left[1 + \frac{\epsilon_{\rho\omega}s}{48\pi^2 g_{\omega\gamma}^2}\right. \\
&\times \left.\int_{4M_\pi^2}^\infty \mathrm{d}s'\frac{\sigma_\pi^3(s')|F_\pi^V(s')|^2}{s'(s' - s - i\epsilon)}\right].
\end{aligned} \tag{D.20}
$$

This is our final result for a dispersive representation of $F_{P\gamma^*\gamma^*}(s,0)$ that includes corrections from ρ–ω mixing in a consistent manner, with crucial ingredient the function $P(s)$ as determined by the $P \to \pi^+\pi^-\gamma$ spectrum (3.4). In particular, from the limit $s \to \infty$ one can read off the sum rule

$$
\begin{aligned}
F_{P\gamma\gamma} &= \frac{1 - \epsilon_{\rho\omega}}{48\pi^2}\int_{4M_\pi^2}^\infty \mathrm{d}s'\,\sigma_\pi^3(s')P(s')|F_\pi^V(s')|^2 \\
&+ F_{P\gamma\gamma}\,w_{P\omega\gamma} \\
&\times \left[1 - \frac{\epsilon_{\rho\omega}}{48\pi^2 g_{\omega\gamma}^2}\int_{4M_\pi^2}^\infty \mathrm{d}s'\frac{\sigma_\pi^3(s')|F_\pi^V(s')|^2}{s'}\right].
\end{aligned} \tag{D.21}
$$

The isoscalar part of the TFF also involves a contribution from the ϕ, which simply amounts to adding

$$
F_{P\gamma^*\gamma^*}^\phi(s,0) = \frac{F_{P\gamma\gamma}\,w_{P\phi\gamma}\,s}{M_\phi^2 - s - iM_\phi\Gamma_\phi} \tag{D.22}
$$

to the right-hand side of Eq. (D.20) (and $F_{P\gamma\gamma}\,w_{P\phi\gamma}$ to the one of Eq. (D.21)). The combination of Eqs. (D.20) and (D.22) is the form (2.3) gitven in the main text.

As a final cross check, we show that Eq. (D.20) reproduces the correct VMD limit. To this end, we first approximate the dispersive integrals by their narrow-width limit, in analogy to Eq. (C.12). The second integral already takes VMD form, while for the former we need $|P(M_\rho^2)|$. This quantity can be

---

[6] This can be done more rigorously by using a smeared-out version of the δ-function instead, but the results are identical. See also the discussion leading to Eq. (C.12).

related to $\Gamma(P \to \rho\gamma)$ by integrating Eq. (3.4) and again replacing the integral by its narrow-width limit. In this way, we can remove $|P(M_\rho^2)|$ in favor of $w_{P\rho\gamma}$, see Eq. (D.8), and using the VMD relations $g_{\rho\pi\pi} = 1/g_{\rho\gamma}$, $g_{\rho\gamma} = 3g_{\omega\gamma}$, we obtain

$$
\begin{aligned}
F_{P\gamma^*\gamma^*}^{\text{VMD}}(s, 0) = F_{P\gamma\gamma} \Bigg[1 &+ \left(1 + \frac{\epsilon_{\rho\omega}s}{M_\omega^2 - s - iM_\omega\Gamma_\omega} \right) \\
&\times \frac{w_{P\rho\gamma}s}{M_\rho^2 - s - iM_\rho\Gamma_\rho} \\
&+ \frac{w_{P\omega\gamma}s}{M_\omega^2 - s - iM_\omega\Gamma_\omega} \\
&\times \left(1 + \frac{9\epsilon_{\rho\omega}s}{M_\rho^2 - s - iM_\rho\Gamma_\rho} \right) \Bigg],
\end{aligned} \qquad \text{(D.23)}
$$

in agreement with the expected VMD result.

References

1. J. Wess, B. Zumino, Phys. Lett. B **37**, 95 (1971)
2. E. Witten, Nucl. Phys. B **223**, 422 (1983)
3. I. Larin et al. [PrimEx-II Collaboration], Science **368**, 506 (2020)
4. S.L. Adler, Phys. Rev. **177**, 2426 (1969)
5. J.S. Bell, R. Jackiw, Nuovo Cim. A **60**, 47 (1969)
6. W.A. Bardeen, Phys. Rev. **184**, 1848 (1969)
7. J. Bijnens, A. Bramon, F. Cornet, Phys. Rev. Lett. **61**, 1453 (1988)
8. J.L. Goity, A.M. Bernstein, B.R. Holstein, Phys. Rev. D **66**, 076014 (2002). arXiv:hep-ph/0206007
9. B. Ananthanarayan, B. Moussallam, JHEP **05**, 052 (2002). arXiv:hep-ph/0205232
10. K. Kampf, B. Moussallam, Phys. Rev. D **79**, 076005 (2009). arXiv:0901.4688 [hep-ph]
11. H. Leutwyler, Nucl. Phys. B Proc. Suppl. **64**, 223 (1998). arXiv:hep-ph/9709408
12. T. Feldmann, P. Kroll, B. Stech, Phys. Rev. D **58**, 114006 (1998). arXiv:hep-ph/9802409
13. T. Feldmann, P. Kroll, B. Stech, Phys. Lett. B **449**, 339 (1999). arXiv:hep-ph/9812269
14. T. Feldmann, Int. J. Mod. Phys. A **15**, 159 (2000). arXiv:hep-ph/9907491
15. R. Escribano, J.-M. Frère, JHEP **06**, 029 (2005). arXiv:hep-ph/0501072
16. R. Escribano, S. Gonzàlez-Solís, P. Masjuan, P. Sánchez-Puertas, Phys. Rev. D **94**, 054033 (2016). arXiv:1512.07520 [hep-ph]
17. K. Ottnad, C. Urbach [ETM Collaboration], Phys. Rev. D **97**, 054508 (2018). arXiv:1710.07986 [hep-lat]
18. L. Gan, B. Kubis, E. Passemar, S. Tulin, Phys. Rep. **945**, 2191 (2022). arXiv:2007.00664 [hep-ph]
19. P.A. Zyla et al. [Particle Data Group], PTEP **2020**, 083C01 (2020)
20. T. Aoyama et al., Phys. Rep. **887**, 1 (2020). arXiv:2006.04822 [hep-ph]
21. T. Aoyama, M. Hayakawa, T. Kinoshita, M. Nio, Phys. Rev. Lett. **109**, 111808 (2012). arXiv:1205.5370 [hep-ph]
22. T. Aoyama, T. Kinoshita, M. Nio, Atoms **7**, 28 (2019)
23. A. Czarnecki, W. J. Marciano, A. Vainshtein, Phys. Rev. D **67**, 073006 (2003). arXiv:hep-ph/0212229 [Erratum: Phys. Rev. D **73**, 119901 (2006)]
24. C. Gnendiger, D. Stöckinger, H. Stöckinger-Kim, Phys. Rev. D **88**, 053005 (2013). arXiv:1306.5546 [hep-ph]
25. M. Davier, A. Hoecker, B. Malaescu, Z. Zhang, Eur. Phys. J. C **77**, 827 (2017). arXiv:1706.09436 [hep-ph]
26. A. Keshavarzi, D. Nomura, T. Teubner, Phys. Rev. D **97**, 114025 (2018). arXiv:1802.02995 [hep-ph]
27. G. Colangelo, M. Hoferichter, P. Stoffer, JHEP **02**, 006 (2019). arXiv:1810.00007 [hep-ph]
28. M. Hoferichter, B.-L. Hoid, B. Kubis, JHEP **08**, 137 (2019). arXiv:1907.01556 [hep-ph]
29. M. Davier, A. Hoecker, B. Malaescu, Z. Zhang, Eur. Phys. J. C **80**, 241 (2020). arXiv:1908.00921 [hep-ph]. [Erratum: Eur. Phys. J. C **80**, 410 (2020)]
30. A. Keshavarzi, D. Nomura, T. Teubner, Phys. Rev. D **101**, 014029 (2020). arXiv:1911.00367 [hep-ph]
31. B.-L. Hoid, M. Hoferichter, B. Kubis, Eur. Phys. J. C **80**, 988 (2020). arXiv:2007.12696 [hep-ph]
32. A. Kurz, T. Liu, P. Marquard, M. Steinhauser, Phys. Lett. B **734**, 144 (2014). arXiv:1403.6400 [hep-ph]
33. K. Melnikov, A. Vainshtein, Phys. Rev. D **70**, 113006 (2004). arXiv:hep-ph/0312226
34. G. Colangelo, M. Hoferichter, M. Procura, P. Stoffer, JHEP **09**, 091 (2014). arXiv:1402.7081 [hep-ph]
35. G. Colangelo, M. Hoferichter, B. Kubis, M. Procura, P. Stoffer, Phys. Lett. B **738**, 6 (2014). arXiv:1408.2517 [hep-ph]
36. G. Colangelo, M. Hoferichter, M. Procura, P. Stoffer, JHEP **09**, 074 (2015). arXiv:1506.01386 [hep-ph]
37. P. Masjuan, P. Sánchez-Puertas, Phys. Rev. D **95**, 054026 (2017). arXiv:1701.05829 [hep-ph]
38. G. Colangelo, M. Hoferichter, M. Procura, P. Stoffer, Phys. Rev. Lett. **118**, 232001 (2017). arXiv:1701.06554 [hep-ph]
39. G. Colangelo, M. Hoferichter, M. Procura, P. Stoffer, JHEP **04**, 161 (2017). arXiv:1702.07347 [hep-ph]
40. M. Hoferichter, B.-L. Hoid, B. Kubis, S. Leupold, S.P. Schneider, Phys. Rev. Lett. **121**, 112002 (2018). arXiv:1805.01471 [hep-ph]
41. M. Hoferichter, B.-L. Hoid, B. Kubis, S. Leupold, S.P. Schneider, JHEP **10**, 141 (2018). arXiv:1808.04823 [hep-ph]
42. A. Gérardin, H.B. Meyer, A. Nyffeler, Phys. Rev. D **100**, 034520 (2019). arXiv:1903.09471 [hep-lat]
43. J. Bijnens, N. Hermansson-Truedsson, A. Rodríguez-Sánchez, Phys. Lett. B **798**, 134994 (2019). arXiv:1908.03331 [hep-ph]
44. G. Colangelo, F. Hagelstein, M. Hoferichter, L. Laub, P. Stoffer, Phys. Rev. D **101**, 051501 (2020). arXiv:1910.11881 [hep-ph]
45. G. Colangelo, F. Hagelstein, M. Hoferichter, L. Laub, P. Stoffer, JHEP **03**, 101 (2020). arXiv:1910.13432 [hep-ph]
46. T. Blum, N. Christ, M. Hayakawa, T. Izubuchi, L. Jin, C. Jung, C. Lehner, Phys. Rev. Lett. **124**, 132002 (2020). arXiv:1911.08123 [hep-lat]
47. G. Colangelo, M. Hoferichter, A. Nyffeler, M. Passera, P. Stoffer, Phys. Lett. B **735**, 90 (2014). arXiv:1403.7512 [hep-ph]
48. M. Hoferichter, T. Teubner, Phys. Rev. Lett. **128**, 112002 (2022). arXiv:2112.06929 [hep-ph]
49. S. Borsanyi et al., Nature **593**, 51 (2021). arXiv:2002.12347 [hep-lat]
50. C. Lehner, A.S. Meyer, Phys. Rev. D **101**, 074515 (2020). arXiv:2003.04177 [hep-lat]
51. A. Crivellin, M. Hoferichter, C.A. Manzari, M. Montull, Phys. Rev. Lett. **125**, 091801 (2020). arXiv:2003.04886 [hep-ph]
52. A. Keshavarzi, W.J. Marciano, M. Passera, A. Sirlin, Phys. Rev. D **102**, 033002 (2020). arXiv:2006.12666 [hep-ph]
53. B. Malaescu, M. Schott, Eur. Phys. J. C **81**, 46 (2021). arXiv:2008.08107 [hep-ph]
54. G. Colangelo, M. Hoferichter, P. Stoffer, Phys. Lett. B **814**, 136073 (2021). arXiv:2010.07943 [hep-ph]
55. G.W. Bennett et al. [Muon $g-2$ Collaboration], Phys. Rev. D **73**, 072003 (2006). arXiv:hep-ex/0602035
56. B. Abi et al. [Muon $g-2$ Collaboration], Phys. Rev. Lett. **126**, 141801 (2021). arXiv:2104.03281 [hep-ex]

57. T. Albahri et al. [Muon $g − 2$ Collaboration], Phys. Rev. D **103**, 072002 (2021). arXiv:2104.03247 [hep-ex]

58. T. Albahri et al. [Muon $g − 2$ Collaboration], Phys. Rev. A **103**, 042208 (2021). arXiv:2104.03201 [hep-ex]

59. T. Albahri et al. [Muon $g − 2$ Collaboration], Phys. Rev. Accel. Beams **24**, 044002 (2021). arXiv:2104.03240 [physics.acc-ph]

60. V. Pauk, M. Vanderhaeghen, Eur. Phys. J. C **74**, 3008 (2014). arxiv:1401.0832 [hep-ph]

61. I. Danilkin, M. Vanderhaeghen, Phys. Rev. D **95**, 014019 (2017). arXiv:1611.04646 [hep-ph]

62. F. Jegerlehner, Springer Tracts Mod. Phys. **274**, 1 (2017)

63. M. Knecht, S. Narison, A. Rabemananjara, D. Rabetiarivony, Phys. Lett. B **787**, 111 (2018). arXiv:1808.03848 [hep-ph]

64. G. Eichmann, C.S. Fischer, R. Williams, Phys. Rev. D **101**, 054015 (2020). arXiv:1910.06795 [hep-ph]

65. P. Roig, P. Sánchez-Puertas, Phys. Rev. D **101**, 074019 (2020). arXiv:1910.02881 [hep-ph]

66. E.-H. Chao, R.J. Hudspith, A. Gérardin, J.R. Green, H.B. Meyer, K. Ottnad, Eur. Phys. J. C **81**, 651 (2021). arXiv:2104.02632 [hep-lat]

67. J. Leutgeb, A. Rebhan, Phys. Rev. D **101**, 114015 (2020). arXiv:1912.01596 [hep-ph]

68. L. Cappiello, O. Catà, G. D'Ambrosio, D. Greynat, A. Iyer, Phys. Rev. D **102**, 016009 (2020). arXiv:1912.02779 [hep-ph]

69. M. Hoferichter, P. Stoffer, JHEP **05**, 159 (2020). arXiv:2004.06127 [hep-ph]

70. J. Lüdtke, M. Procura, Eur. Phys. J. C **80**, 1108 (2020). arXiv:2006.00007 [hep-ph]

71. J. Bijnens, N. Hermansson-Truedsson, L. Laub, A. Rodríguez-Sánchez, JHEP **10**, 203 (2020). arXiv:2008.13487 [hep-ph]

72. J. Bijnens, N. Hermansson-Truedsson, L. Laub, A. Rodríguez-Sánchez, JHEP **04**, 240 (2021). arXiv:2101.09169 [hep-ph]

73. M. Zanke, M. Hoferichter, B. Kubis, JHEP **07**, 106 (2021). arXiv:2103.09829 [hep-ph]

74. I. Danilkin, M. Hoferichter, P. Stoffer, Phys. Lett. B **820**, 136502 (2021). arXiv:2105.01666 [hep-ph]

75. G. Colangelo, F. Hagelstein, M. Hoferichter, L. Laub, P. Stoffer, Eur. Phys. J. C **81**, 702 (2021). arXiv:2106.13222 [hep-ph]

76. F. Stollenwerk, C. Hanhart, A. Kupść, U.-G. Meißner, A. Wirzba, Phys. Lett. B **707**, 184 (2012). arXiv:1108.2419 [nucl-th]

77. C. Hanhart, A. Kupść, U.-G. Meißner, F. Stollenwerk, A. Wirzba, Eur. Phys. J. C **73**, 2668 (2013). arXiv:1307.5654 [hep-ph]. [Erratum: Eur. Phys. J.C **75**, 242 (2015)]

78. B. Kubis, J. Plenter, Eur. Phys. J. C **75**, 283 (2015). arXiv:1504.02588 [hep-ph]

79. S. Holz, J. Plenter, C.W. Xiao, T. Dato, C. Hanhart, B. Kubis, U.-G. Meißner, A. Wirzba, Eur. Phys. J. C **81**, 1002 (2021). arXiv:1509.02194 [hep-ph]

80. C. Hanhart, Phys. Lett. B **715**, 170 (2012). arXiv:1203.6839 [hep-ph]

81. M. Ablikim et al. [BESIII Collaboration], Phys. Rev. Lett. **120**, 242003 (2018). arXiv:1712.01525 [hep-ex]

82. R. Omnès, Nuovo Cim. **8**, 316 (1958)

83. C. Hanhart, S. Holz, B. Kubis, A. Kupść, A. Wirzba, and C. W. Xiao, Eur. Phys. J. C **77**, 98 (2017). arXiv:1611.09359 [hep-ph]. [Erratum: Eur. Phys. J. C **78**, 450 (2018)]

84. L.-Y. Dai, X.-W. Kang, U.-G. Meißner, X.-Y. Song, D.-L. Yao, Phys. Rev. D **97**, 036012 (2018). arXiv:1712.02119 [hep-ph]

85. M.N. Achasov et al., J. Exp. Theor. Phys. **101**, 1053 (2005). arXiv:hep-ex/0506076

86. M.N. Achasov et al., J. Exp. Theor. Phys. **103**, 380 (2006). arXiv:hep-ex/0605013

87. R.R. Akhmetshin et al. [CMD-2 Collaboration], Phys. Lett. B **527**, 161 (2002). arXiv:hep-ex/0112031

88. R. R. Akhmetshin et al. [CMD-2 Collaboration], Phys. Lett. B **578**, 285 (2004). arXiv:hep-ex/0308008

89. R.R. Akhmetshin et al., JETP Lett. **84**, 413 (2006). arXiv:hep-ex/0610016

90. R.R. Akhmetshin et al. [CMD-2 Collaboration], Phys. Lett. B **648**, 28 (2007). arXiv:hep-ex/0610021

91. B. Aubert et al. [BaBar Collaboration], Phys. Rev. Lett. **103**, 231801 (2009). arXiv:0908.3589 [hep-ex]

92. J.P. Lees et al. [BaBar Collaboration], Phys. Rev. D **86**, 032013 (2012). arXiv:1205.2228 [hep-ex]

93. F. Ambrosino et al. [KLOE Collaboration], Phys. Lett. B **670**, 285 (2009). arXiv:0809.3950 [hep-ex]

94. F. Ambrosino et al. [KLOE Collaboration], Phys. Lett. B **700**, 102 (2011). arXiv:1006.5313 [hep-ex]

95. D. Babusci et al. [KLOE Collaboration], Phys. Lett. B **720**, 336 (2013). arXiv:1212.4524 [hep-ex]

96. A. Anastasi et al. [KLOE-2 Collaboration], JHEP **03**, 173 (2018). arXiv:1711.03085 [hep-ex]

97. A. Abele et al. [Crystal Barrel Collaboration], Phys. Lett. B **402**, 195 (1997)

98. G. D'Agostini, Nucl. Instrum. Methods A **346**, 306 (1994)

99. R.D. Ball, L. Del Debbio, S. Forte, A. Guffanti, J.I. Latorre, J. Rojo, M. Ubiali [NNPDF Collaboration], JHEP **05**, 075 (2010). arXiv:0912.2276 [hep-ph]

100. S.E. Müller, G. Venanzoni, Private communication, as quoted in Ref. [27] (2018)

101. M. Ablikim et al. [BESIII Collaboration], Phys. Lett. B **753**, 629 (2016). arXiv:1507.08188 [hep-ex]

102. M.N. Achasov et al. [SND Collaboration], JHEP **01**, 113 (2021). arXiv:2004.00263 [hep-ex]

103. J.P. Lees et al. [BaBar Collaboration], Phys. Rev. D **104**, 112003 (2021). arXiv:2110.00520 [hep-ex]

104. D. Stamen, D. Hariharan, M. Hoferichter, B. Kubis, P. Stoffer, arXiv:2202.11106 [hep-ph]

105. G. Abbiendi et al., arXiv:2201.12102 [hep-ph]

106. M. Ablikim et al. [BESIII Collaboration], arXiv:1912.11208 [hep-ex]

107. M.N. Achasov et al., Phys. Rev. D **68**, 052006 (2003). arXiv:hep-ex/0305049

108. M. Ablikim et al. [BESIII Collaboration], Phys. Rev. D **92**, 012001 (2015). arXiv:1504.06016 [hep-ex]

109. S. Holz, Bachelor's thesis, Bonn University (2016)

110. S.P. Schneider, B. Kubis, F. Niecknig, Phys. Rev. D **86**, 054013 (2012). arXiv:1206.3098 [hep-ph]

111. M. Hoferichter, B. Kubis, D. Sakkas, Phys. Rev. D **86**, 116009 (2012). arXiv:1210.6793

112. H.J. Behrend et al. [CELLO Collaboration], Z. Phys. C **49**, 401 (1991)

113. H. Aihara et al. [TPC/Two Gamma Collaboration], Phys. Rev. Lett. **64**, 172 (1990)

114. G. Mbianda Njencheu, PhD thesis, Old Dominion University (2017)

115. L. Heijkenskjöld [A2 Collaboration], EPJ Web Conf. **199**, 02013 (2019)

116. L. Heijkenskjöld [A2 Collaboration], EPJ Web Conf. **212**, 03004 (2019)

117. S. Ropertz, C. Hanhart, B. Kubis, Eur. Phys. J. C **78**, 1000 (2018). arXiv:1809.06867 [hep-ph]

118. L. von Detten, F. Noël, C. Hanhart, M. Hoferichter, B. Kubis, Eur. Phys. J. C **81**, 420 (2021). arXiv:2103.01966 [hep-ph]

119. M. Hoferichter, B. Kubis, S. Leupold, F. Niecknig, S.P. Schneider, Eur. Phys. J. C **74**, 3180 (2014). arXiv:1410.4691 [hep-ph]

120. M. Hoferichter, B. Kubis, M. Zanke, Phys. Rev. D **96**, 114016 (2017). arXiv:1710.00824 [hep-ph]

121. F. Niecknig, B. Kubis, S.P. Schneider, Eur. Phys. J. C **72**, 2014 (2012). arXiv:1203.2501 [hep-ph]